Climate Dynamics (1998) 14:545–569

V. Moron · R. Vautard · M. Ghil

Trends, interdecadal and interannual oscillations in global sea-surface temperatures

Received: 19 December 1996 / Accepted: 8 November 1997

Abstract This study aims at a global description of climatic phenomena that exhibit some regularity during the twentieth century. Multi-channel singular spectrum analysis is used to extract long-term trends and quasi-regular oscillations of global sea-surface temperature (SST) fields since 1901. Regional analyses are also performed on the Pacific, (Northern and Southern) Atlantic, and Indian Ocean basins. The strongest climatic signal is the irregular long-term trend, characterized by overall warming during 1910–1940 and since 1975, with cooling (especially of the Northern Hemisphere) between these two warming intervals. Substantial cooling prevailed in the North Pacific between 1950 and 1980, and continues in the North Atlantic today. Both cooling and warming are preceded by SST anomalies of the same sign in the subpolar North Atlantic. Near-decadal oscillations are present primarily over the North Atlantic, but also over the South Atlantic and the Indian Ocean. A 13–15-y oscillation exhibits a seesaw pattern between the Gulf-Stream region and the North-Atlantic Drift and affects also the tropical Atlantic. Another 7–8-y oscillation involves the entire double-gyre circulation of the North Atlantic, being mostly of one sign across the basin, with a minor maximum of opposite sign in the subpolar gyre and the major maximum in the northwestern part of the subtropical gyre. Three distinct interannual signals are found, with periods of about 60–65, 45 and 24–30 months. All three are strongest in the tropical Eastern Pacific. The first two extend throughout the whole Pacific and still exhibit some consistent, albeit weak, patterns in other ocean basins. The latter is weaker overall and has no consistent signature outside the Pacific. The 60-month oscillation obtains primarily before the 1960s and the 45-month oscillation afterwards.

V. Moron[1]
Instituto per lo Studio delle Metodologie Geofisiche, CNR, I-40129 Bologna, Italy

R. Vautard (✉)
Laboratoire de Météorologie Dynamique du CNRS, Ecole Normale Supérieure, 24 rue Lhomond, F-75231 Paris Cedex 05, France
E-mail: vautard@ella.ens.fr

M. Ghil
Department of Atmospheric Sciences and Institute of Geophysics and Planetary Physics, University of California, Los Angeles, CA 90095-1565, USA

Present address:
[1] Centre Aixois de Géographie Physique (CAGE), CNRS/Université de Provence, F-13621 Aix en Provence, France

1 Introduction and motivation

1.1 Background

Many authors have studied long-term instrumental temperature records to separate possible anthropogenic climate change from natural climate variability (e.g., Ghil and Vautard 1991; Folland et al. 1992; Mann and Park 1993; Allen and Smith 1994; Schlesinger and Ramankutty 1994a, b, 1995; Plaut et al. 1995; Nicholls et al. 1996; Parker et al. 1994, 1996). All these studies concluded that a significant, but irregular warming trend has occurred on a global scale since 1850. The global trend is fairly flat from the middle of the nineteenth century till 1910, followed by increases of over 0.1 °C/decade in combined land- and sea-surface temperatures during 1910–1940 and the last two decades. These two warming episodes were separated by mild cooling, especially in the Northern Hemispheric (Jones et al. 1986a, b; Folland et al. 1992; Parker et al. 1994, 1996). A reversal of interhemispheric contrast occurred between 1951–60 and 1981–90, with the Northern Hemisphere becoming the colder of the two. Recent global warming has been associated by some authors with abrupt changes in the North Pacific around 1976 or with a gradual warming of the tropical Pacific (Pan

and Oort 1990; Trenberth 1990; Tanimoto et al. 1993; Trenberth and Hurrell 1994; Graham 1994; Kerr 1994; Latif and Barnet 1994, 1995), as well as with other regional phenomena (Folland et al. 1986; Kumar et al. 1996; Hurrell 1996).

This irregular trend, and the identification of any anthropogenic or other external effects on it, is obscured by the presence of natural climate variability, traditionally interpreted as red noise (Hasselmann 1976; Mitchell 1976). More recently, it has been argued that his variability has some regularity imbedded into it. The existence of such regularity on the interannual time scale is fairly well established and attributed largely, if not exclusively, to an instability of the coupled ocean-atmosphere system in the tropical Pacific (Philander 1990; Rasmusson et al. 1990). Of late, two distinct periodicities,near 4–6 y and 2–3 y (Rasmusson and Carpenter 1982; Barnett 1991; Allen 1992; Keppenne and Ghil 1992; Mann and Park 1994; Jiang et al. 1995), have been associated with this El-Niño/Southern-Oscillation (ENSO) phenomenon. The evidence for similar regularity on the near-decadal and interdecadal time scale (Ghil and Vautard 1991; Allen and Smith 1994; Mann et al. 1995b, Mann and Park 1996; Plaut et al. 1995) is more difficult to establish, due to the shortness of instrumental temperature and sea-level (Unal and Ghil 1995) records. We review, therefore, in the next subsection, previous studies of long temperature records, their data sets, methods and results.

1.2 A review of previous studies

Table 1 summarizes the main studies published since 1990 and directly concerned with the analysis of observed climatic signals, using various statistical methods. In this table, we only consider studies of instrumental measurements of global climate or proxies deduced from regularly kept diaries (like the Central England Temperature Index of Manley 1953, 1974, as used by Plaut et al. 1995 and Allen and Smith 1996, or the drought/flood index in East China, as used by Liang et al. 1995 but not paleoclimatic proxies such as tree rings, coral reefs or marine-sediment varves (e.g., Fritts et al. 1979; Cook 1995; Mann et al. 1995b; Quinn et al. 1996; Biondi et al. 1997). The data used in these studies can be divided into two groups: (1) univariate indices, assumed to be representative of large-scale climatic variability; the most common indices considered are the Southern Oscillation Index (SOI) and suitable averages of continental or global temperature records (see Folland et al. 1992 or Nicholls et al. 1996 for a review); and (2) multivariate, gridded data sets; the most common ones are sea- or land-surface temperatures. Jones et al. (1986a, b), Bottomley et al. (1990), and Woodruff et al. (1987) describe, respectively, the temperature data sets of the University of East Anglia's Climate Research Unit (CRU), of the UK Meteorological Office (UKMO), and the Comprehensive Ocean-Atmosphere Data Set (COADS); the latter also contains surface winds (Woodruff et al. 1987). Univariate analyses extend, in general, over longer time intervals than the multivariate ones, while the majority of multivariate analyses investigate only the post-World War 2 period.

Extraction of multiple time scale signals has been carried out using various statistical methods which can, essentially, be divided into five groups. In the first one, composite analyses and running means of an index or a field are considered (e.g., Kawamura 1994; Kushnir 1994; Allan et al. 1995); in the latter case, the field is often spatially prefiltered by projection onto the leading empirical orthogonal functions (EOFs). Several time intervals of prescribed length are averaged and differences tested using a classical *t*-test. The main advantage of this method is its simplicity but it suffers from the subjectivity of the chosen length for intervals of presumably homogeneous behavior and the fact that the presence of red, rather than white noise degrades the results of classical *t*-tests (Zwiers and von Storch 1995). In the second group, the data are prefiltered in time by using a prescribed, fixed filter, and the patterns associated with each frequency so detected are investigated using principal component analysis (PCA: Tanimoto et al. 1993) or complex PCA (Barnett 1991). The main disadvantage of this method is once again the subjectivity of the choice of, in this case, the arbitrarily prescribed time filter. An improvement on this method is to use advanced nonparametric spectral techniques, such as the multi-taper method, to prefilter the data and then study teleconnections related to the extracted frequencies by singular-value decomposition (Mann and Park 1993, 1994).

In the third group, principal oscillation patterns (Hasselmann 1988; Ooms 1988; von Storch et al. 1988; Penland and Ghil 1993; Penland 1996) fit a multivariate autoregressive process of order one to a time series of fields. This method is data-adaptive, but assumes that the dynamics generating the fields is linear and stable. In the fourth group, the orthogonal wavelet transform, introduced recently into climate studies (Meyers et al. 1993; Gu and Philander 1995; Lau and Weng 1995; Mak 1995; Yiou et al. 1995; Wang and Wang 1996), has the advantage of automatically tracking changes in the frequency, as well as the amplitude, of the oscillations being investigated but noisy systems remain difficult to study and error bars are not easily available. The fifth group is formed by singular-spectrum analysis (SSA: Vautard and Ghil 1989; Vautard et al. 1992; Dettinger et al. 1995a), Monte-Carlo SSA (MC-SSA: Allen 1992; Allen and Smith 1996) and multi-channel SSA (MSSA: Kimoto et al. 1991; Keppenne and Ghil 1993; Plaut and Vautard 1994). These methods are data-adaptive, i.e., the bandwidth and shape of the filters is not provided by the user but by the data. They are all extensions of PCA to delay-

Table 1 Summary of studies published (since 1990) based on uni- and multivariate analysis of large-scale observed climatic signals over a long time interval (40 y or longer) that include an explicit distinction between different time scales

References	Method: U for univariate and M for multivariate	Physical nature of the data and coverage in time and space
Rasmusson et al. (1990)	SSA (U)	Gridded SSTs and surface winds over the Indo-Pacific area
Barnett (1991)	Prefiltering and CPCA (M)	Gridded pressure and tropical SST (1950–1988)
Elsner and Tsonis (1991)	SSA (U)	IPCC (1856–1990)
Allen (1992)	Monte Carlo SSA (U)	IPCC (1861–1990) and SOI (1935–1985)
Ropelewski et al. (1992)	Filtering, correlations and harmonic analysis (M)	Gridded SST and surface winds (1949–1987)
Deser and Blackmon (1993)	Prefiltering and PCA (M)	Gridded SST and atmospheric data (Nov–March 1900–1989)
Mann and Park (1993)	Multi-taper spectral analysis and teleconnections (M)	Gridded surface temperatures (1891–1990)
Allen and Smith (1994)	Monte Carlo SSA (U) and regression with significant oscillations (M)	IPPC (1861–1990) and SST
Graham (1994)	Canonical correlations, composites (M)	Gridded data (SST, surface winds, OLR, …) in Northern and Equatorial Pacific (1950–1986)
Kawamura (1994)	PCA and running mean (M)	Gridded SST (1950–1988)
Kushinr (1994)	Composite analysis and running mean (M)	Gridded SST in Northern Atlantic (1900–1987)
Mann and Park (1994)	Multi-taper spectra analysis and complex SVD (M)	Gridded surface-air temperature (1890–1990)
Parker et al. (1994)	Composite analysis on non-overlapping decadal periods (M)	Gridded surface-air temperatures (1891–1990)
Schlesinger and Ramankutty (1994)	SSA (U) (residuals from a trend computed using a simple hemispheric coupled model)	IPCC (1858–1992) and "large-scale" boxes
Tanimoto et al. (1994)	Prefiltering and PCA (M)	Gridded SST on North Pacific (1950–1990)
Trenberth and Hurrel (1994)	Filtering, correlations and composite analyses (M)	PNA index (1924–1992)
Allen et al. (1995)	Composite analysis on 21-years non-overlapping periods (M)	Gridded SST and surface winds during Jan–Mar 1900–1983 over the Indian Ocean
Dettinger et al. (1995b)	MSSA (M)	Gridded surface-air temperatures over the United States (1910–1987)
Gu and Philander (1995)	Wavelet transform (U)	Gridded SST and surface winds indices (1870–1988)
Jiang et al. (1995)	MSSA (M)	Gridded SST and winds on equatorial Pacific (1950–1990)
Lau and Weng (1995)	Wavelet transform (U)	Northern Hemisphere Surface Temperature Index (1854–1993)
Liang et al. (1995)	Spectral analysis (U) and Hovmöller diagram	Annual drought/flood index over East China (1470–1988)
Mak (1995)	Wavelet transform (U)	SST over the Pacific (1949–1992)
Mann et al. (1995b)	Frequency-domain SVD (M)	Instrumental and proxy data (1400–1960)
Mehta and Delworth (1995)	Power spectra and SSA (U)	Gridded SST on Tropical Atlantic (1889–1988)
Plaut et al. (1995)	SSA (U)	Central England Temperatures (1659–1990)
Schlesinger and Ramankutty (1995)	SSA (U) s(residuals from a trend computed using a simple hemispherical coupled model)	IPCC (1858–1992)
Unal and Ghil (1995)	SSA (U) and MSSA (M)	Relative Sea-level height (1807–1988)
Wang (1995)	Composite analysis, filters and PCA (M)	Gridded SST and surface winds (1956–1992)
Wang and Ropelewski (1995)	SSA, filters and PCA (M)	Gridded SST (1860–1989)
Allen and Robertson (1996)	Monte Carlo M-SSA (M)	3-month running mean Tropical Pacific SST (1951–1992)
Allen and Smith (1996)	Monte Carlo SSA (U)	IPCC (1858–1993), SOI (1866–1993), Central England temperatures (1659–1993)

coordinate phase space (Broomhead and King 1986a, b).

Reviews of all the advanced spectral method mentioned in the last two paragraphs include Ghil and Yiou (1996), Yiou et al. (1996), and Ghil and Taricco (1997). Their relative strengths and weaknesses, in particular, are summarized in tabular form by the latter. Additional information, including portable computer

codes and visualization tools for some of the methods, can be found on the World Wide Web at http//www.atmos.ucla.edu/tcd.

The conclusions of the studies in Table 1 are fairly consistent for the interannual variability (2–10 y) but controversial for interdecadal variability. The major interannual periodicities are 2–3 y, 4–6 y (Rasmusson et al. 1990; Barnett 1991; Ghil and Vautard 1991; Allen 1992; Keppenne and Ghil 1992; Allen and Smith 1994; Jiang et al. 1995; Unal and Ghil 1995), and 7–8 y (Mann and Park 1993, 1994; Dettinger et al. 1995b; Plaut et al. 1995). Many observational and modeling studies have provided some evidence that both the quasi-biennial (QB: 2–3 y) and quasi-quadrennial (4–6 y) peaks are related to ENSO. The alternation of "weak" and "strong" annual cycles in the Indo-Pacific domain (Meehl 1987, 1992) provides substantial QB variability in various climatic parameters, particularly over this area. A list of such parameters includes Indian rainfall (Parthasarathy et al. 1993), Indian surface wind (Terray 1995), equatorial Pacific SST and surface wind (Rasmusson et al. 1990; Ropelewski et al. 1992), global continental precipitation (Lau and Sheu 1988), and the zonal circulation of the tropics (Moron et al. 1995).

Recent modeling studies have explored in greater depth the interaction between the annual cycle and the intrinsic ENSO instability (Jin et al. 1994, 1996; Tziperman et al. 1994; Chang et al. 1995), producing a plausible physical explanation for both the QB (4/2 y) and quasi-quadrennial (4/1 y) peaks, as well as of a tentatively identified 16–17-month (4/3 y) peak (Jiang et al. 1995; Robertson et al. 1995). Observed interannual variability at 6–9 y has been related to a mid-latitude oceanic mechanism by Speich et al. (1995).

Several authors have also investigated the possible impact of ENSO-related variability around the Atlantic ocean (Hastenrath and Covey 1978; Nicholson and Entekhabi 1986; Aceituno 1988; Pisciottano et al. 1994) but correlations seem overall weaker than for the Indo-Pacific domain. A quasi-quadrennial coupled ocean-atmosphere mode, similar to the Pacific ENSO, has been reported by Zebiak (1993) in the tropical Atlantic, but is not self-sustained. Delecluse et al. (1994) showed that the Atlantic "El niño" of 1984 was strongly forced by the previous Pacific El Niño of 1982–83. Janicot et al. (1996) concluded that the relationship between West-African rainfall and SOI is not consistent, with no reliable relationship between 1950 and 1970 and a significant positive one after this date. Latif et al. (1996) argued, through observations and numerical simulations, that an analog of the coupled Pacific ENSO mode, tentatively dubbed "El Hermanito," does exist in the Atlantic basin, but with a shorter period (about 30 months) and weaker amplitude, owing to the reduced size of the Equatorial Atlantic. Another mode, with a periodicity of 7–8 y, seems independent of ENSO (Mann and Park 1993, 1994) and is most prominent over the North Atlantic (Plaut et al. 1995). Outside the Atlantic basin, the effects of ENSO, either regional or globally averaged, have been documented fairly convincingly (Ropelewski and Halpert 1987; Ghil and Vautard 1991; Pan and Oort 1990; Ropelewski et al. 1992).

At decadal and multi-decadal time scales, no satisfactory consensus has emerged so far. The main problem with signals having periods longer than 10 y is the poor temporal coverage: 10–15 realizations, at best, since the beginning of regular large-scale instrumental records. The significance of such oscillations is marginal when tested against a red-noise null hypothesis (Allen 1992; Allen and Smith 1996). The bidecadal oscillations reported by Ghil and Vautard (1991) in both the CRU and IPCC (Houghton et al. 1990) time series of global-mean and hemispheric temperatures have, therefore, been argued over by Elsner and Tsonis (1991) and Allen et al. (1992), and the North-Atlantic 65–70-y oscillation claimed by Schlesinger and Ramankutty (1994a, b, 1995) has been questioned by Elsner and Tsonis (1994) and Allen and Smith (1996). Still, Allen and Smith (1994) and Mann and Park (1993, 1994) confirm, using different spectral methods and data sets (see Table 1), the existence of bidecadal oscillations, mainly over the high latitudes of the North Atlantic where the major source of deep-water formation is located (Broecker 1987; Ghil et al. 1987; Schlosser et al. 1991; Read and Gould 1992).

An important mechanism of interdecadal climate variability is provided by changes in the oceans' thermohaline circulation. Idealized, as well as fairly realistic models of the oceans' general circulation, whether uncoupled (Weaver et al. 1991; Weisse et al. 1994; Chen and Ghil 1995; Greatbatch and Zhang 1995; Rahmstrof 1995) or coupled to the atmosphere (Delworth et al. 1993; Chen and Ghil 1996) or to sea ice (Mysak et al. 1991) have produced regular or irregular oscillations with dominant periods between 10 and 100 y. The period of such a model oscillation can depend on many poorly known parameters and hence a better way of evaluating the model against data is by the comparison of the spatial patterns associated with the oscillations. Besides the evidence, in both the models and the data, for interdecadal oscillations being most prominent around the North Atlantic (Mann and Park 1993, 1994; Plaut et al. 1995), some evidence also exists for near-decadal oscillations occurring in the tropical Atlantic (Allen 1992; Allen and Smith 1994; Mehta and Delworth 1995) and in the Sahel's annual rainfall (Moron 1997).

The purpose of this study is to clarify further the spatial patterns associated with the regular, nearly periodic components of interannual and interdecadal climate variability, as reflected by the World Ocean's sea-surface temperatures (SSTs). We apply the MSSA technique to a fairly long data set (1901–1994) of monthly-sampled SSTs. Such an application so far has been carried out only over the equatorial Pacific sector (Jiang et al. 1995). The advantage of MSSA is to take

Table 2 List of acronyms

Acronym	Nature	Definition
COADS	Data set	Comprehensive Ocean Atmospheric Data Set
CRU	Data source	Climate Research Unit
ENSO	Phenomenon	El Niño-Southern Oscillation
EOF	Methodological	Empirical orthogonal function
IPCC	Data source	Intergovernmental Panel on Climatic Change
MC-SSA	Methodological	Monte Carlo singular spectrum analysis
MOHSST	Data set	Monthly historical SSTs
MSSA	Methodological	Multivariate (or multi-channel) SSA
NAO	Phenomenon	North Atlantic Oscillation
PCA	Methodological	Principal component analysis
QB	Phenomenon	Quasi-biennial
RC	Methodological	Reconstructed component
S-EOF	Methodological	Spatial EOF
SLP	Time series (uni- or multivariate)	Sea-level pressure
SIO	Time series (univariate)	Southern Oscillation Index
S-PC	Methodological	Spatial principal component
SSA	Methodological	Singular-spectrum analysis
SST	Time series (multivariate)	Sea-surface temperature
ST-EOF	Methodological	Space-time EOF
ST-PC	Methodological	Space-time principal component
SVD	Methodological	Singular-value decomposition
UKMO	Data source	UK Meteorological Office

into account at the same time, in a data-adaptive and robust fashion, both space- and time-correlations, and to identify therewith standing as well as travelling signals, over a wide range of time scales (Plaut and Vautard 1994). The emphasis is on determining the global or basin-wide character of this low-frequency, relatively regular variability and on comparing our results with those obtained by other methods and with different data (sub)sets.

The data are presented and the methods are reviewed in Sect. 2. An Appendix provides technical details and Table 2 a list of acronyms. We apply MSSA to the global SST field in Sect. 3 and to regional SST fields in Sect. 4. Results are summarized and discussed in Sect. 5.

2 Data and methodology

2.1 The data set

The UKMO monthly SSTs (Bottomley et al. 1990) were extracted from the MOHSST5 data base (Folland and Parker 1995) over the 1901–1994 time interval. Modern, systematic recording of observations started in 1853 and the global data bases COADS and MOHSST begin respectively in 1854 and 1856 (Woodruff et al. 1987; Bottomley et al. 1990). Data density in the Meteorological Office's main data bank, which is the basis of the MOHSST data set, jumps abruptly from about 10 000 per year to 50 000 per year at the turn of the century, hence our decision to use data for this century only (compare Dettinger et al. 1995b for a similar compromise between length of interval and data density). The instrumental biases owing to changes in measurement technique (buckets versus engine-intake water) have been removed for the years preceding 1941 (Folland and Parker 1995). The corrections used for this data set depend on season, location and the history of instrumentation. The data after 1941 were considered by the UKMO as homogeneous (Parker et al. 1994) and have therefore not been corrected.

The basic data we worked with were provided to us as anomalies relative to the 1951–80 mean annual cycle on a $5^\circ \times 5^\circ$ spatial grid. We averaged these data further on a $10^\circ \times 10^\circ$ grid, thus favoring spatio-temporal coverage, which becomes therewith almost continuous from 40 °S to 65 °N, over (possibly unreliable) spatial details. A $10^\circ \times 10^\circ$ box is retained if at least one of the four $5^\circ \times 5^\circ$ boxes inside it has data. Boxes having less than 50% of data coverage, so defined, over the entire January 1901–December 1994 interval were rejected. The number of remaining $10^\circ \times 10^\circ$ boxes is 330.

Missing data for those boxes that were retained were filled with a realization of a suitably chosen noise process that is white in time, as proposed by Unal and Ghil (1995). Several realizations of this "interpolation noise" were generated, and the results on the trend and oscillatory components were found to be similar from one realization to another. This illustrates the robustness of the interpolation and analysis procedure, which is conservative in the sense that is overestimates the noise variance in the entire time series and thus underestimates the signal-to-noise ratio of the climate process that generates it.

2.2 MSSA and related methods

MSSA has been extensively presented in many papers (Broomhead and King 1986b; Kimoto et al. 1991; Keppenne and Ghil 1993; Plaut and Vautard 1994; Vautard 1995; Jiang et al. 1995; Unal and Ghil 1995; Da Costa and Vautard 1996). We recall here briefly the procedure and some essential terminology, but refer to Plaut and Vautard (1994) for technical details. The SST anomalies are first spatially filtered by a classical PCA, and a few leading eigenmodes are retained. The truncation is performed here by a scree test on the eigenvalue spectra (O'Lenic and Livezey 1988) and we checked that our results do not depend in any substantial way on this truncation. The eigenvectors of this spatial PCA are called the spatial EOFs (S-EOFs) and their associated time-dependent projection coefficients the spatial principal components (S-PCs). These coefficients form the "channels" to be analyzed by MSSA.

MSSA consists in diagonalizing the lag-covariance matrix of the multi-channel time series, with lags ranging from 0 to $M-1$; $W = M\Delta t$ is called the window width, with $\Delta t = 1$ month being the sampling interval. The eigenvectors of this matrix, which are lag-sequences of maps, are called the space-time EOFs (ST-EOFs), and their associated projection coefficients, which are scalar time series, are called the space-time principal components (ST-PCs). MSSA allows the identification of robust oscillations which are reflected by a phase quadrature between a pair of ST-PCs, as well as between the corresponding ST-EOFs: the latter are the data-adaptive basis functions, which correspond for an oscillation to a space-time sine-and-cosine pair (or to the statistical counterpart of a pair of eigensolutions of a wave operator). The phase quadrature between ST-PCs is used in order to identify reliably oscillatory pairs. Following Plaut and Vautard (1994), we consider two statistical eigenmodes to form an oscillatory pair when the first extrema, on either side of the origin, of the lag-correlation function between the two ST-PCs

under examination have absolute values that both exceed 0.6; this criterion is slightly more stringent than Plaut and Vautard's (1994) who set the threshold at 0.5. We also restrict the analysis to eigenmodes of high variance, whose order does not exceed 15, and focus on periods larger than one year.

Following the single-channel formalism of Ghil and Vautard (1991) and Vautard et al. (1992), Plaut and Vautard (1994) defined space-time reconstructed components (RCs), that are versions of the original sequence of maps filtered by projecting onto subsets of ST-EOFs. Unlike the ST-PCs, whose length is shorter than that of the raw time series by the window width W, the ST-RCs are equal in length to the original signal and can, therefore, be used to determine the, slowly changing, phase and amplitude indices of a given oscillation. The mathematical formulation of the phase index is an improved version of Plaut and Vautard's (1994), and given in the Appendix (see also Da Costa and Vautard 1996 and Dettinger and Ghil 1997). For each oscillating pair, the phase index $\theta(t)$, which varies between 0 and 2π, describes the life cycle of the oscillation, whether intermittent or sustained. One can think of this index as being defined on the unit circle. In order to describe concisely and objectively the spatial patterns of the oscillation's life cycle, the RCs with index falling within a given 45°-sector of the unit circle are averaged. In this manner, 8 phase composites are formed, and their associated patterns can be displayed in a single multi-panel figure (see the Appendix for technical details).

The MSSA windows used here are of width $W = 72$, 120 and 168 months; some computations with $W = 240$ months have also been carried out. The choice of window width represents a compromise between the maximal period that can be detected, which equals W, and the reliability of this detection, which varies like $1/W$. The use of multiple windows to check the robustness of the results is highly recommended (Dettinger et al. 1995a). The first window width was chosen because many studied (Ropelewski and Halpert 1987; Barnett 1991) concluded that ENSO-related interannual variability is concentrated below 6 y. This window allows one to investigate oscillations between 16 and 72 months (see Vautard et al. 1992). The other windows are used for the investigation of sub- and interdecadal variability, of 7–15 y.

Several climatic signals required additional testing due to the relative closeness of the period of interest to the total length of the time series. Analyses were then also performed with univariate MC-SSA, following Allen (1992). In this case, each channel is tested individually against the two null hypotheses of "red noise" and "red noise + signal." First, an ensemble of 100 "surrogate" time series, each consisting of realization of an auto-regressive process of order 1, AR(1) noise, is generated. If a pair of eigenelements beats the "red-noise" null hypothesis by falling outside this 1000-member ensemble's spectra at a preset confidence level (with respect to a two-side test), then the reconstructed signal associated with this pair is considered to be significant. If so, the second null hypothesis is that the observed time series consists of this signal being contaminated by an AR(1) noise process, and another 1000-member ensemble is generated, by adding AR(1) realizations to the signal. The same preset confidence level (e.g., 95%) is applied to testing the presence of any additional signal in the channel of interest (Allen and Smith 1996).

3 Interannual and interdecadal variability of the World Ocean

3.1 Spatial EOFs (S-EOFs)

In this section, we present the results of the analysis performed on the global SSTs. Eight S-EOFs, describing 24% of the total variance, are retained for subsequent analysis according to the scree test of Sect. 2.2 (see also Table 3). S-EOF 1 (not shown) represents the ENSO pattern; the highest positive loadings are over the equatorial Eastern Pacific, with slightly lower positive values along North America's west coast and the Peruvian coast and over the entire tropical ocean, while the highest negative values occur over the North-Central Pacific and over the South Pacific convergence zone (SPCZ). The modest negative loading over the Equatorial Atlantic agrees with Kawamura's (1994) result. S-PC 1 (not shown) is a good index of the major warm and cold (El Niño and La Niña) events in the tropical Pacific, with a higher noise level before 1941, as suggested by the need to preprocess the earlier data. The second EOF is also related to ENSO, but with relatively higher loadings over the Central and tropical Eastern Pacific, and almost uniform loadings over the Atlantic and Indian oceans. Subsequent EOFs describe more regional features.

3.2 Trend and oscillating pairs

The main characteristics of the oscillating pairs identified by MSSA are summarized in Table 4 for windows of 72, 120 and 168 months; the table also gives the results of the regional analyses that will be described in Sect. 4. For each window, two-to-three interannual oscillations are identified, with major peaks near 61–65, 43 and 25–27 months. These periods are in rough agreement with previous studies, and are presumed therewith to be all related to the ENSO phenomenon. The maximum entropy spectra (see Plaut and Vautard 1994 for details) of the corresponding ST-PCs are plotted in Fig. 1, for $W = 72$, $W = 120$, and $W = 168$ months. The results of these three spectral analyses are used in the last two columns of Table 4.

Table 3 Percentage of variance described by the ten leading spatial principal components (S-PCs) for the SST over the World Ocean as well as for the five-separate ocean basins considered. Each row corresponds to a given basin, while the columns represents the S-PC order. The leading components retained for each basin are in boldface

Domain	1	2	3	4	5	6	7	8	9	10
World	**7.8**	**5.0**	**2.5**	**2.1**	**1.8**	**1.7**	**1.6**	**1.6**	1.4	1.4
Pacific	**11.9**	**5.4**	**3.6**	**2.9**	**2.7**	**2.5**	1.9	1.8.	1.8	1.7
Atlantic	**9.4**	**5.4**	**5.0**	**4.9**	**4.3**	3.5	3.2	2.8	2.6	2.4
North Atlantic	**11.8**	**8.7**	**8.5**	6.2	5.6	4.5	3.8	3.3	3.1	2.6
South Atlantic	**16.7**	**10.3**	6.5	5.5	4.9	4.6	4.0	3.9	3.2	3.0
Indian	**13.3**	**5.9**	**5.2**	**4.4**	**4.0**	3.5	3.3	3.2	3.1	2.7

Table 4 Main characteristics of the oscillating pairs identified by MSSA for the various geographic domains (first column) and the three windows (72, 120 and 168 months, second column). The third column contains the pair order, the fourth contains the total fraction of variance (%) described by the pair, the fifth contains the peak period, and the last column gives the variance described by the pair at the peak frequency, as calculated from the maximum entropy spectra. Sometimes, the oscillating pair has two or three spectral peaks, which are then listed in order of importance and separated by slashes

Region	Window W (month)	Pair	Total variance (%)	Period (month)	Variance at peak (%)
World Ocean	72	3–4	11	65	54
		9–10	4	25	46
	120	3–4	8	61	68
		12–13	3	27	55
		4–5	6	63	64
	168	6–7	5	43	72
		14–15	2	27	48
Pacific Ocean	72	2–3	15	65	71
		7–8	5	24	60
	120	2–3	10	63	74
		9–10	4	30	52
		2–3	8	63	69
		6–7	7	43	68
	168	9–10	5	83/56/39	41/27/17
		11–12	3	36/26	39/37
		14–15	3	30	38
Atlantic Ocean	72	7–8	3	40	39
	120	7–8	3	91	40
		10–11	2	42	37
	168	9–10	2	91	47
		11–12	2	43	54
North Atlantic Ocean	72	11–12	3	28	35
	120	14–15	2	25	41
	168	3–4	5	154	64
		7–8	3	91	45
South Atlantic Ocean	72	4–5	7	44	65
		9–10	4	20	64
		7–8	4	65/39	40/33
	120	10–11	3	29	83
		12–13	3	23	68
		8–9	3	63/43	37/25
	168	10–11	2	28	60
		12–13	2	33	52
Indian Ocean	120	6–7	3	40	44
	168	8–9	2	43	63
		11–12	2	34	55

The pure-trend component ST-PC1 (see Fig. 1a) contains a major part of the variance (about 20% for $W = 72$ months). For $W = 72$ months, the second component mixes trend and variability around 50 months. The extension of the window to 120 months (Fig. 1b) clearly separates the trend (now given by components 1 and 2) from frequencies that can be captured within the latter window.

For all windows, the dominant oscillating pair 3–4 is associated with a spectral peak near 65 months. The peak is sharper for $W = 120$ months than for $W = 72$ months, due to the increased resolution (Vautard et al. 1992). For $W = 168$ months (Fig. 1c), a new low-frequency oscillation is resolved, with a period of about 43 months. This oscillation corresponds to the quasi-quadrennial mode described by Jiang et al. (1995). As noted also by these authors, it is difficult to identify the low-frequency ENSO mode originally described by Rasmusson et al. (1990) with a single well-defined spectral peak. The discrepancy between the period of the main peak reported by Jiang et al. (1995), equal there to about 52 months. and the 43 months here, could be due to the fact that they worked with data covering a shorter time span (1950–1990).

To investigate this point, we display in Fig. 2 the reconstruction of the low-frequency ENSO oscillations based on pair 3–4 (63 months), for $W = 72$ months, which does not distinguish between the two lowest-frequency modes, and for $W = 168$ months, which captures the two as pairs 4–5 (63 months) and 6–7 (43 months); the particular scalar time series displayer is channel 1 i.e., S-PC1 filtered by the ST-RC pairs just mentioned. In the lumped reconstruction ($W = 72$ months), there is a clear frequency shift after the

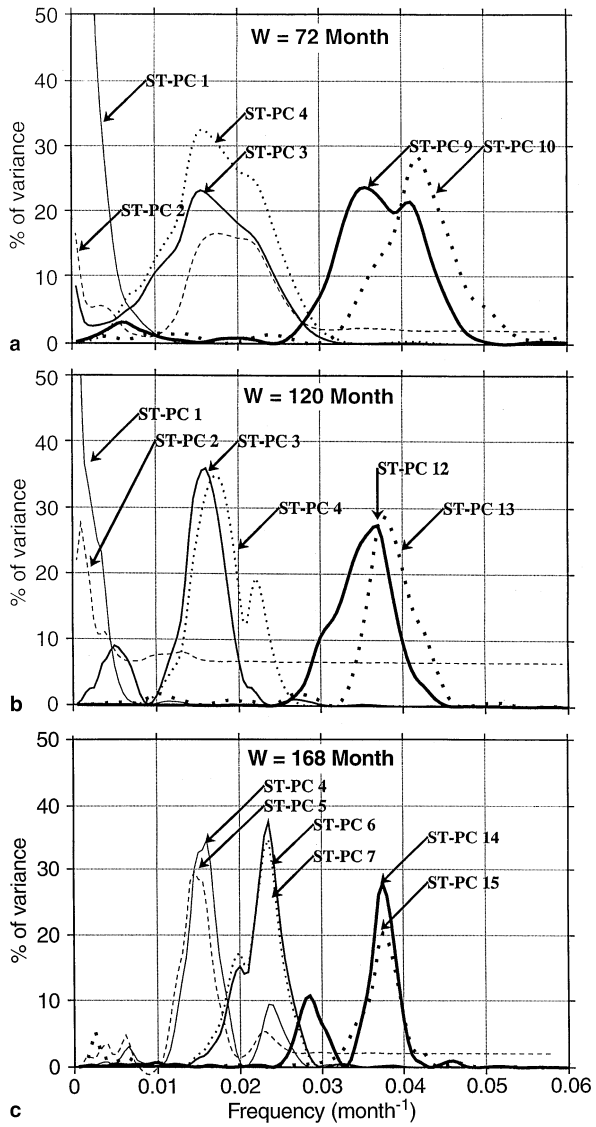

Fig. 1a–c Fraction of variance, as a function of the frequency, described by various ST-PCs of the World Ocean's SST field for: **a** $W = 72$, **b** $W = 120$, and **c** $W = 168$ months. The *curves* displayed are estimated by dividing the spectra of the ST-PCs by the total spectrum. The spectra are estimated by the multi-channel version of the maximum entropy method, as described by Plaut and Vautard (1994). See *legends* on the graphs

sixties: periods of about 60 months, or even longer, are found before 1960, while the dominant period is about 45 months during the decades since. The separated reconstruction ($W = 168$ months) shows that the slower oscillation (pair 4–5, dashed) dominates in the early part of the century, while the faster one (pair 6–7, dotted) dominates towards the end of the century, and that the transition in 1960 is fairly sharp. Wang and Wang (1996) obtained similar conclusions, using single-channel wavelet analysis on SOI and, separately, on an SST anomaly index.

Typically, in an oscillator, whether linear or nonlinear, the period is a smooth function of the model parameters. This dependence was studied in some detail for an ENSO model linearized about an annually averaged state by Neelin and Jin (1993). The only phenomenon that entails a sharp change in period, such as the historic shift from a quasi-quinquennial to a quasi-quadrennial period observed here around 1960, is the Devil's staircase scenario (Jin et al. 1994, 1996; Tziperman et al. 1994; Chang et al. 1995). Under this scenario, the coupled ocean-atmosphere system in the tropical Pacific can frequency-lock most easily to integer multiples of the seasonal cycle's period. This conjecture is also confirmed by the fact that ST-EOFs associated with the two lowest-frequency modes are quite similar (not shown, but see discussion in Jiang et al. 1995).

The next oscillation is a QB oscillation represented by the pair of ST-PCs 9–10 ($M = 72$), 12–13 ($M = 120$) or 14–15 ($M = 168$), with a main spectral peak of 25–27 months. The variance captured by this oscillation is close to 1/3 of the previous one, quasi-quinquennial ($M = 72$ or $M = 120$) or quasi-quadrennial ($M = 168$). In the frequency domain, this oscillation represents about 50% of the variance at its peak value, meaning that the QB oscillation clearly dominates the noise at slightly over 24 months.

3.3 Spatial characteristics of the slow phenomena

The long-term trend (ST-PCs 1 and 2) is reconstructed using MSSA with $W = 120$ months and projected back

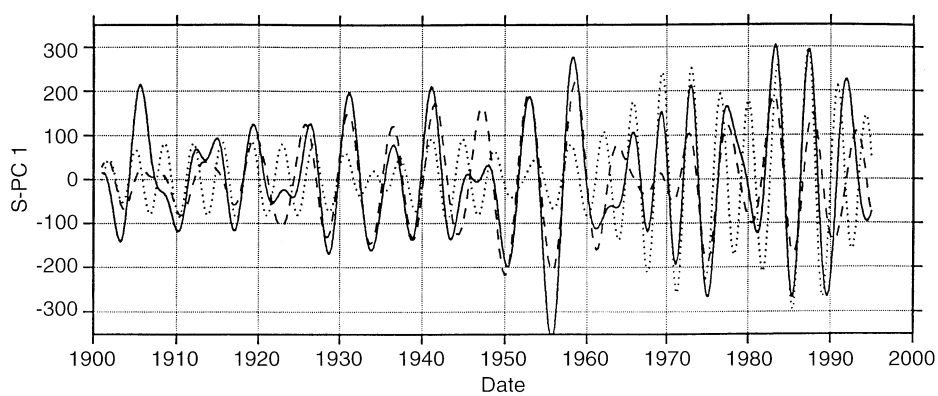

Fig. 2 Reconstructions in channel 1 (i.e., first S-PC) of the 63-month oscillation ($W = 168$ months, *dashed*), the 43-month oscillation ($W = 168$ months, *dotted*) and the single slow mode peaking at 65 months for $W = 72$ months (*solid*). Units are 0.01 °C

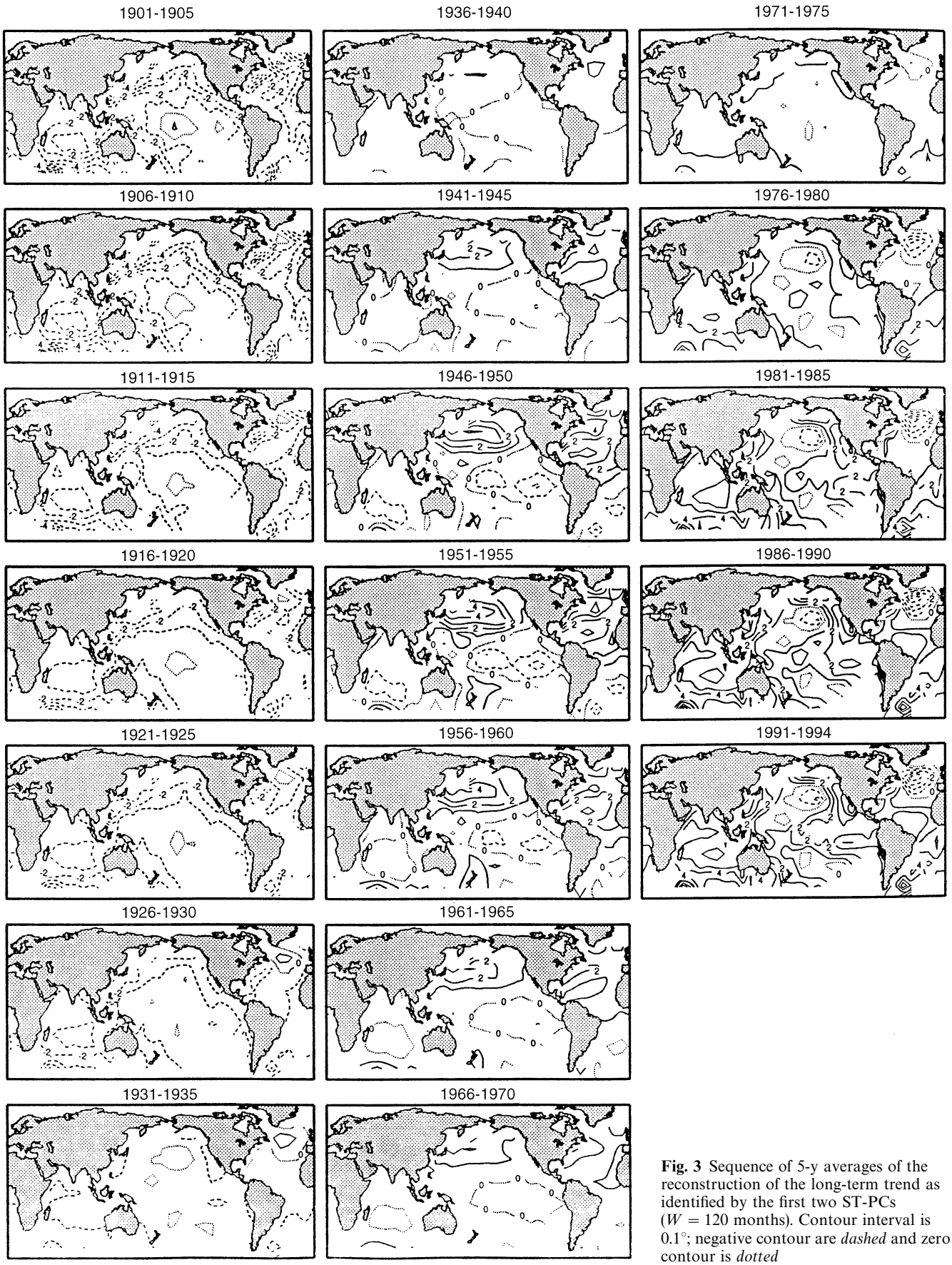

Fig. 3 Sequence of 5-y averages of the reconstruction of the long-term trend as identified by the first two ST-PCs ($W = 120$ months). Contour interval is 0.1°; negative contour are *dashed* and zero contour is *dotted*

onto the leading eight S-EOFs. We display in Fig. 3 the anomaly patterns of successive 5-y averages, from 1901 on, with respect to the data set's 1901–1994 long-term mean. Results for $W = 168$ months (not shown) are fairly similar, since ST-PC 3 in this case does not contribute substantially to the trend, which is still captured by ST-PCs 1 and 2.

The global coldness before 1930 is obvious; the only areas slightly above zero are off the southern tip of Greenland and in the tropical Pacific. Slow warming begins in the twenties over the northwest Atlantic and in the thirties over the North-Central Pacific. This warming extends to the whole Northern Hemisphere during the forties, while much of the Southern Hemisphere remains colder than the long-term mean. The anomaly patterns change abruptly in the seventies (see also Kushnir 1994 and Parker et al. 1994) with a reversal of the interhemispheric contrast: the Northern Hemisphere cools and the Southern one warms. Again, the cooling trend both starts and is strongest south of Greenland. Almost simultaneously, a similar but lesser cooling occurs over the North Pacific.

To clarify further the global, hemispheric and regional trends that can be extracted from Fig. 3, we show the means over the globe and the two hemispheres of the trend ST-RCs in Fig. 4a and four gridpoint evaluations in Fig. 4b. The global trend (heavy solid) exhibits clearly, albeit in a smoother fashion than in previous analyses, based on *a priori*, prescribed filters (e.g., Parker et al. 1996), the global warming during the 1910–1940 and 1975–1994 episodes and flatness in between. It is striking that both hemispheric trends coincide with the global one unit 1920, diverge from it till 1950, with the Northern Hemisphere warmer and the Southern one colder, to intersect again in 1970 and diverge in opposite directions since.

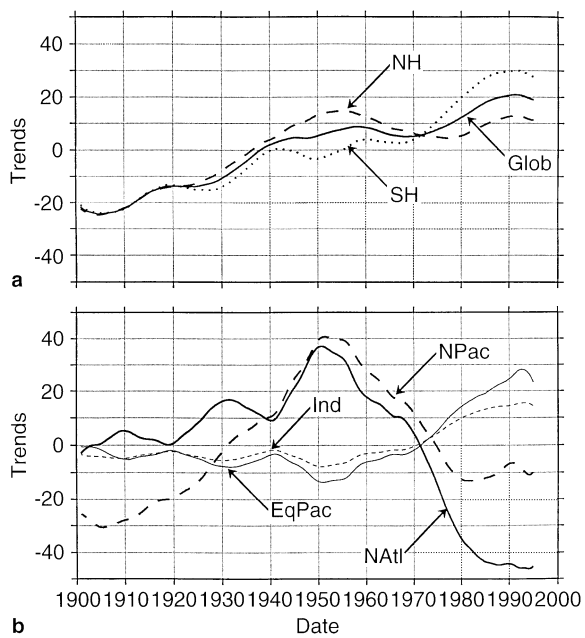

Fig. 4 **a** Global and hemispheric trends obtained from ST-RCs 1–2 ($W = 120$ months). **b** Four local trends obtained from the same ST-RCs: NAtl (35 °W, 55 °N), NPac (165 °W, 45 °N), EqPac (165 °W, 5 °N), and Ind (85 °E, 15 °S). See *legends* on graphs and in text; units are 0.01 °C

The curves in Fig. 4b correspond to the North Atlantic's (35 °W, 55 °N, heavy solid) and North Pacific's (165 °W, 45 °N, heavy dashed) subpolar gyres and to the tropical Indian (85 °E, 5 °S, light dashed) and equatorial Eastern Pacific (115 °W, 5 °N, light solid) oceans. It is clear that the warming starts in the North Atlantic before the North Pacific, but the two evolve in a remarkably similar fashion between 1940 and 1970. The cooling that started for the North Atlantic slightly earlier, in 1950, seems to be flattering out since 1980 for both ocean areas. The trends in the Eastern Pacific and Indian tropical oceans are much less pronounced than the midlatitude trends already noted while they involve much larger area of the globe, and are fairly indistinguishable from each other, expect during the latest decade or so. They are anticorrelated with the northern mid-latitudes, and their recent warming trend is also flattering out over the last few years.

The change in SST, and hence in thermocline depth, in the equatorial Eastern Pacific appears to be particularly sharp just before 1960. This could be a plausible cause for the fairly abrupt change in the dominant period of the low-frequency mode from five to four years, at about this time.

The low-frequency mode and QB oscillations are spatially reconstructed using the phase-compositing technique described in Sect. 2 and in the Appendix. The composites are displayed in Figs. 5 and 6, respectively, for the 72-month window. Phases 1–3 represent their respective contribution to the build-up of a warm event in the tropical Central and Eastern Pacific. For both modes, warm anomalies occur first near the Peruvian coast and then over the whole Pacific Ocean east of 160 °E and along the west coast of the Americas, from Alaska to Chile. The two oscillations patterns are fairly similar over the Pacific Ocean, except that the QB mode is less intense. The main difference lies in the more global character of the low-frequency mode, while the QB mode is essentially confined to the Pacific Ocean (see also Dettinger and Ghil 1997). In the low-frequency mode, the warm phases are also associated with a slightly lagging warmth of the entire Indian Ocean and of the subtropical Atlantic in both hemispheres, while a cold anomaly is observed over the equatorial Atlantic (see also Latif and Barnett 1995 and Lanzante 1996).

The decaying phase of a low-frequency warm event (phase 4–5) is characterized by warm anomalies over tropical regions outside the major perturbation in the tropical Pacific. This relative warming persists over the equatorial Atlantic, while cold anomalies develop everywhere else. The last phase (8), representing the decay of a cold event, is characterized by cold

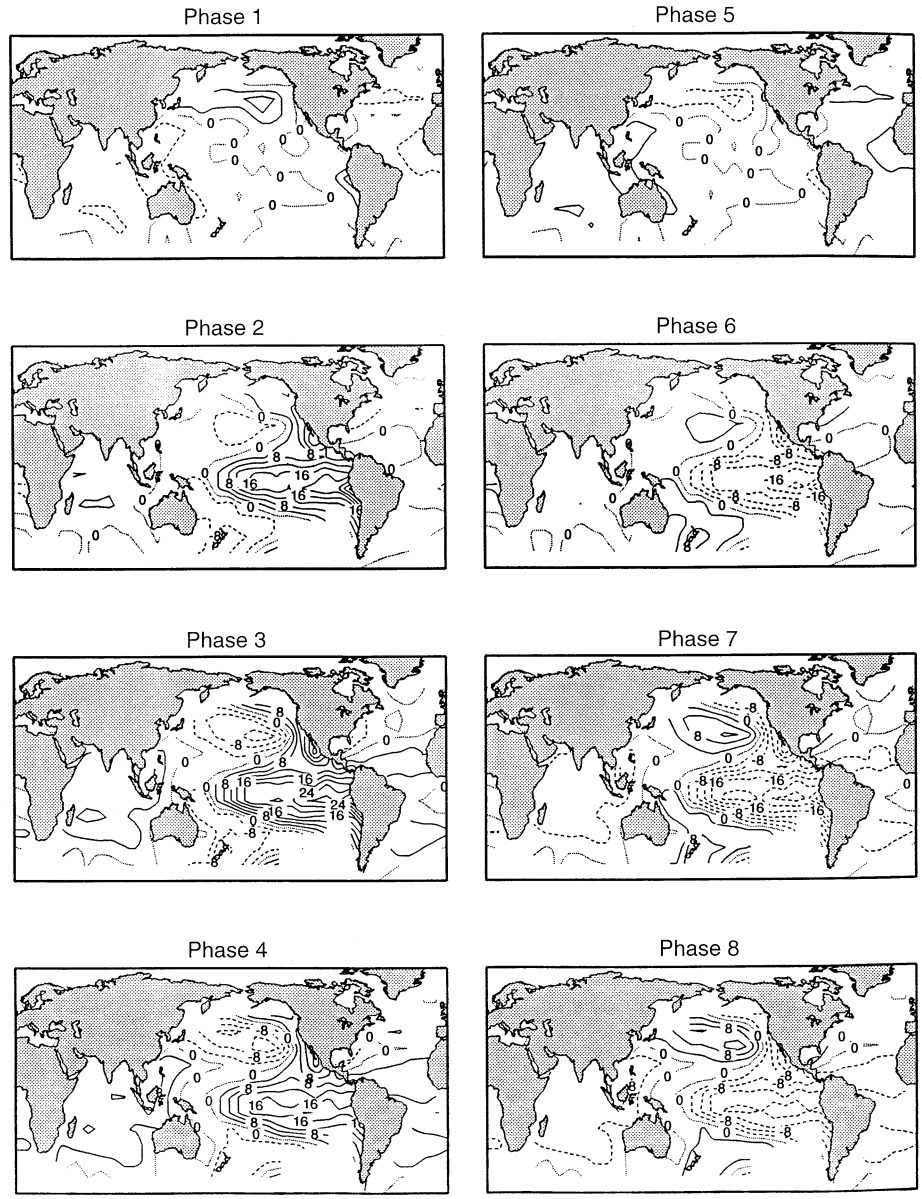

Fig. 5 Life cycle of the low-frequency (quasi-quinquennial) ENSO oscillation ($W = 72$ months), using the phase-compositing technique described in the Appendix, based on ST-RCs 3–4. Contour interval is 0.04 °C

anomalies almost everywhere, except over the mid-latitudes of the Central and Western Pacific, in both hemispheres.

Oscillations with similar periods are obtained when analyzing by single-channel SSA (with the same window width of 72 months) the SOI (Keppenne and Ghil 1992) and the Niño-3 SST index; the latter is obtained from the COADS SST data by averaging over the Niño-3 area. The time behavior of the reconstruction in channel 1 (for global SSTs) is displayed in Fig. 7, together with the corresponding (single-channel) reconstructed oscillations obtained with the SOI and Niño-3 indices. Lag-correlations for the low-frequency signal (labeled QQ in the figure) are maximal when SOI leads the global reconstruction by one month (equaling then -0.81) and when Niño-3 leads it by three months (0.85). The regional ENSO signal thus seems to lead the large-scale, remote signal at this low frequency.

For the QB signal, correlation values are lower: RCs 3–4 for either the SOI or Niño-3 correlate best with channel 1 of global ST-RCs 9–10 synchronously or nearly so: the optimal lag for SOI is 0 and the correlation is -0.58, while it is 0.67 when Niño-3 leads by one month. The full reconstructed signal using both the low-frequency and QB components (RCs 1–4 of either SOI or Niño-3) exhibits the same relationships: the correlation with channel 1 of ST-RCs 3–4 and 9–10 equals -0.76 when SOI leads by one month and 0.78 when Niño-3 leads by two months (see also Dettinger and Ghil 1997 for lead and lag relationships between the tropical SSTs, Northern Hemisphere surface-air temperature and atmospheric CO_2 concentrations.

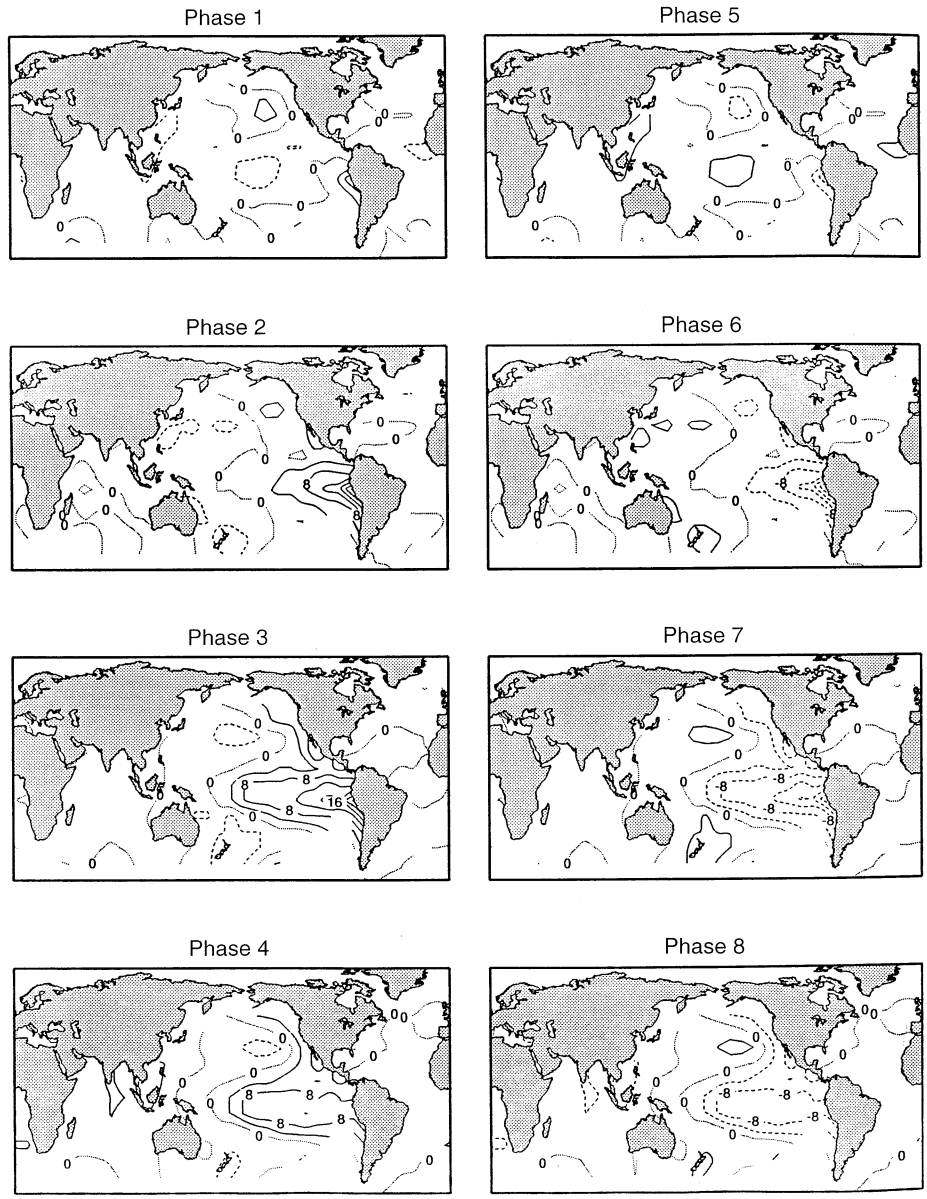

Fig. 6 Same as Fig. 5 for the QB (25-month) oscillation, based on ST-RCs 9–10

4 Regional analyses

4.1 Pacific Ocean

The leading six S-PCs, representing 29% of the total variance of the SSTs over this basin (see Table 3), are retained. MSSA is again applied, with the same three windows as before, to these six channels. Low-frequency and QB oscillations are identified, and the results appear in Table 4. The results are very similar to those of the global analysis, which is not surprising, given the size of the Pacific Ocean. A few minor differences are that the trend occupies only the first component, rather than the first two (for all three windows), and that the variances associated with the leading oscillatory paris are larger, since these interannual oscillations are centered in the Pacific. For $W = 168$ months, the low-frequency mode is split again into two pairs. The QB oscillation is also split into two modes (see also Jiang et al. 1995). This splitting typically happens when windows are much larger than the period of a fairly broad-band oscillation, as explained by Vautard et al. (1992).

The leading ST-PCs do not contain, in the present regional analysis, any regular interdecadal oscillation, even with a window of 168 months. Only one pair (9–10) with very low frequency is detected by the objective selection criterion, but it exhibits 3 peaks, at 83, 56 and 39 months. This component is fairly irregular and unstable when the window width W is varied. ST-PCs 4 and 5 (for $W = 168$ months) also peak at periods longer than 150 months, but do not pass the selection rule.

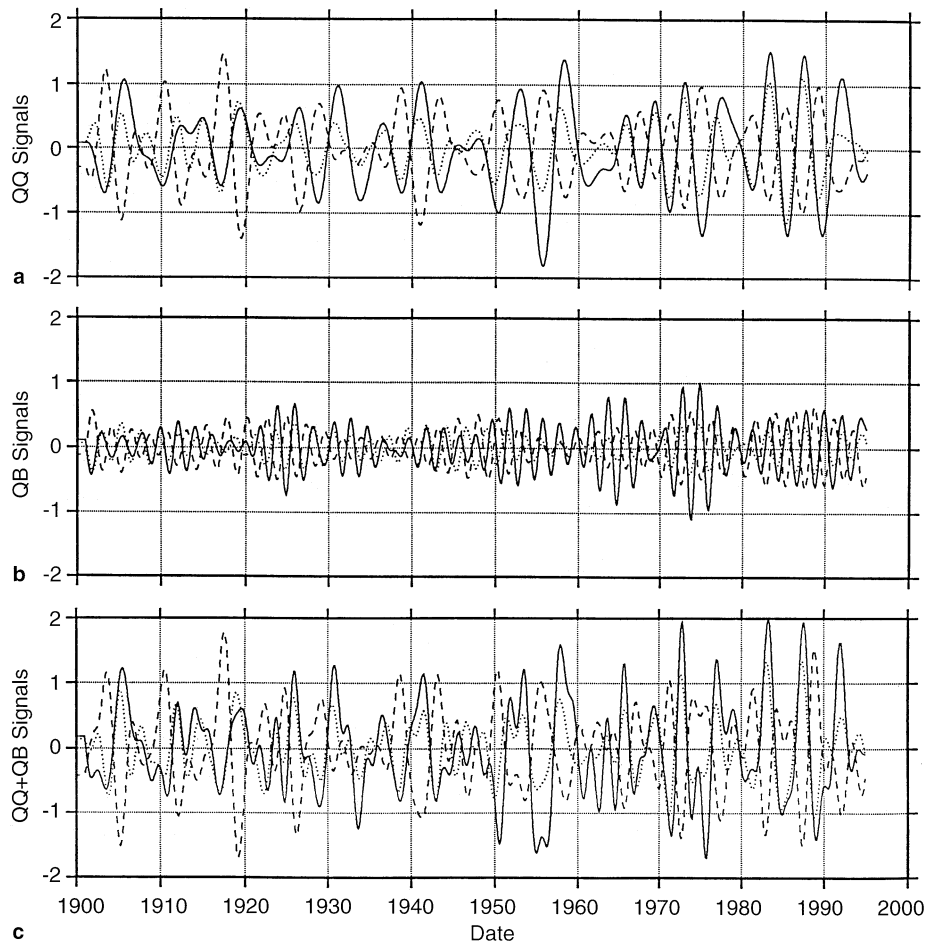

Fig. 7a–c Reconstruction of the ENSO oscillations found in the World-Ocean SSTs (S-PC 1, *solid*), the Niño-3 SSTs (*dotted*) and the SOI (*dashed*), for $W = 72$ months). **a** Low-frequency signals (labeled *QQ*); **b** QB signals; and **c** sum of the reconstructed QQ and QB signals. In order to allow for better comparison between the SOI and SST time series, the data have been normalized to zero mean and unit variance. Note that the amplitude of the Niño-3 signals is not systematically lower during the first half of the century when data coverage was sparser in the Eastern Tropical Pacific; this indicates that our $10^\circ \times 10^\circ$ data set has fairly stationary properties over the time interval of study

Previous studies suggest that North-Pacific SST variability has an important near-decadal or interdecadal component of (Tanimoto et al. 1993; Latif and Barnett 1994; Mann et al. 1995b) and might be due to an oscillation in the Kuroshio's location (Speich et al. 1995). Both Deser and Blackmon (1995) and Zhang et al. (1997) detect an SST pattern centered over the North Pacific that is distinct from the ENSO-related whole-Pacific pattern there (see also Fig. 5) and exhibits broad-band interdecadal variability. To verify whether this broad-band phenomenon has a more regular, narrow-band component, we carried out MSSA on North-Pacific SSTs using five channels and $W = 240$ months. No significant pair with periods longer than the ENSO-related ones was detected, although Biondi et al. (1997) did find 25- and 12-year peaks by applying single-channel SSA to a millennium-long (AD 1117–1992) varved record off the coast of California.

A similar MSSA analysis for the South Pacific, using 3 channels and $W = 240$ months, did detect a significant pair peaking at 105 months, besides the interannual, ENSO-related peaks. This near-decadal peak ($\cong 8.7$ y) could be related to the 7.5-year peak in a two-century-long coral record from Vanuatu (Quinn et al. 1996). The latter record also contained a highly significant 14–15-y peak (see also Ghil and Vautard 1991 and Mann and Park 1994).

4.2 Atlantic Ocean

We keep the leading five S-PCs, which describe 29% of the total variance. The application of MSSA, with the standard three windows used throughout, reveals that near-decadal and interdecadal variability dominates over the Atlantic Ocean. The leading ST-PCs 1–6 (for $W = 72$ and $W = 120$ months) and 1–8 ($W = 168$ months) have associated periods longer than 100 months and describe respectively 37, 34 and 35% of the variance. With a window of 120 or 168 months, one is able to detect a near-decadal oscillation (see Table 4) with a period of about 91 months (pair 7–8 or 9–10). The other oscillation identified has a period near that of the Pacific quasi-quadrennial mode (40–43 months: pair 7–8 for $W = 72$, 10–11 for $W = 120$ and 11–12 for $W = 168$).

The amplitude of the near-decadal oscillation is strongest over the North Atlantic and will be discussed in the next subsection. The quasi-quadrennial

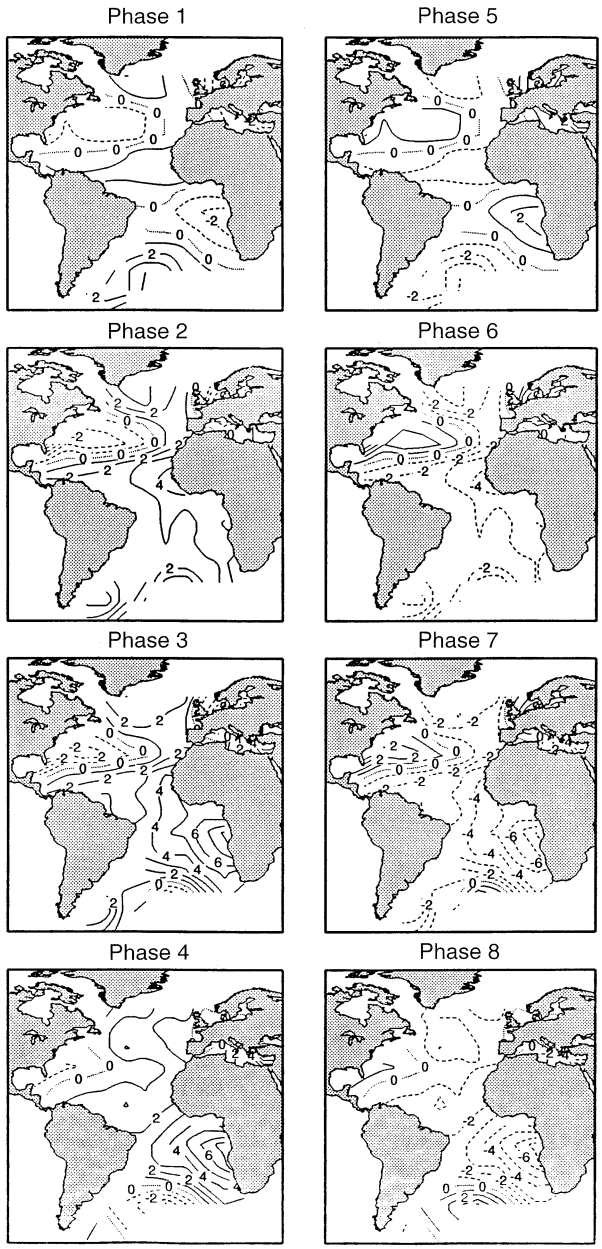

Fig. 8 Phase composites of the quasi-quadrennial signal identified in the Atlantic Ocean's SST data. Contour interval in 0.01 °C

oscillation is of global extent over the Atlantic, and its life cycle is shown in Fig. 8. The evolution of the patterns is roughly the same as for the Atlantic part of the oscillation found with global SSTs (compare with Fig. 5). Its main characteristics include a near-synchronous evolution that involves the equatorial Atlantic and the high latitudes of both hemispheres, in phase opposition to the near-simultaneous evolution of the two midlatitude areas. There is a strong suggestion of the subtropical, anti-cyclonic gyres' SSTs evolving in phase opposition to the adjacent subpolar, cyclonic gyres and the zonally oriented equatorial current system, except that the largest amplitude of the midlatitude pattern in the Southern Hemisphere is associated with the Benguela (and thus possibly the "Atlantic El Niño), rather than the Brazil Current (see also Venegas et al. 1996).

As in the Pacific, this quasi-quadrennial oscillation is standing. The associated SOI reconstruction leads the channel 1 reconstruction of this Atlantic oscillation by 11 months, with a correlation of -0.55; thus low (respectively high) SOI over the Pacific leads to an overall warming (respectively cooling) of the tropical Atlantic about one year later. This result seems to support and refine some of the work cited in Sect. 1.2, by indicating a sharper and stabler connection between the tropical Atlantic and Pacific than documented heretofore. Note finally that a QB mode is detected in our MSSA analysis only at high orders, and thus represents but a small fraction of the variance.

We proceed to study separately the North and South Atlantic because decadal variability exhibits, as we shall see, different behavior in the two basins. The line of separation between the two is not taken along the equator since previous results (Servain 1991; Houghton and Tourre 1992) indicate that the entire Gulf of Guinea is strongly coupled with the South Atlantic's variability. A straight line was drawn therefore between Guyanan and Liberia, at 5 °N, in order to separate the two basins in the subsequent analysis.

4.3 North Atlantic

In this case, 3 channels are retained; they describe 29% of the variance and are well separated from the following ones. S-EOF 1 represents the in-phase variability of the entire basin, with highest loadings from the southern tip of Greenland to the Caribbean. S-EOF 2 exhibits a dipole between the basin's midlatitudes on the one hand and the subpolar and tropical Atlantic on the other. S-EOF 3 describes mainly the variability of the Gulf Stream system.

Table 4 summarizes the oscillations detected. For $W = 168$ months, two major peaks are found near 7.5 and 13 y (pairs 3–4 and 7–8, respectively). More precisely, the interdecadal peak has about equal power at 12.8 and 13.9 y for $W = 168$ months, and larger power at 15.2 y than at 13.9 years (the second largest value, in this case) for $W = 240$ months. QB oscillations are found in this basin, but only when using windows of 72 and 120 months (pairs 11–12 and 14–15, respectively) and far weaker than the two major peaks, near 7.5 and 13–15 y, revealed by the analysis with $W = 168$ months (see Table 4).

The life cycle of the 13–15 year oscillation (Fig. 9) exhibits a striking seesaw, with the two maxima of opposite signs occurring between Cape Hatteras and the Bermudas and due south of the Denmark Straits, near the North Atlantic Drift, respectively. There is some indication of downstream propagation, as the

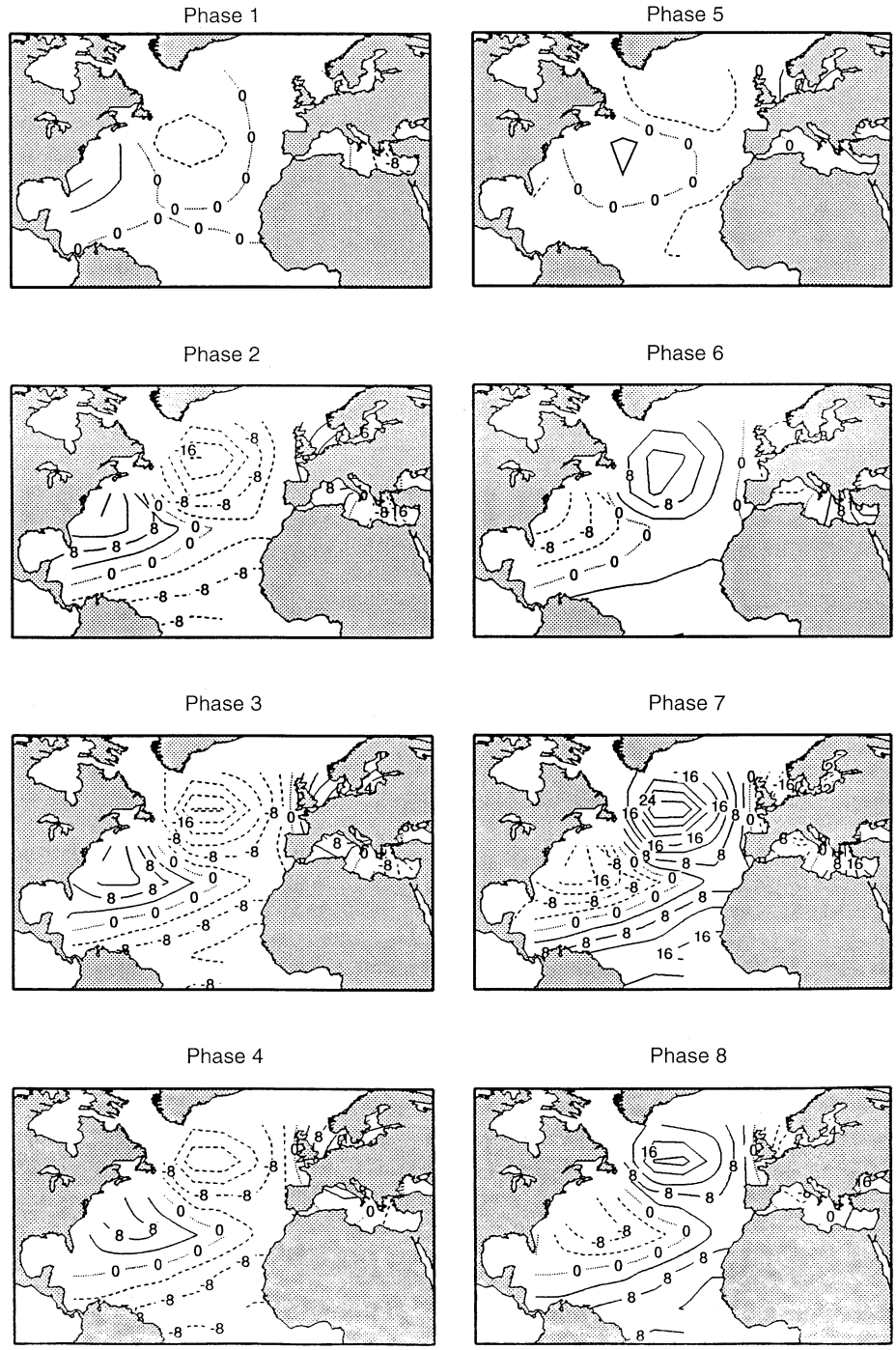

Fig. 9 Phase composites of the interdecadal 13-y oscillation identified over the North Atlantic. Contour interval is 0.04 °C. The southern limit of the analysis domain is 5 °N, while the map extends, for visual convenience, to the Equator

greatest intensification of the second maximum (say from phase 6 to phase 7) occurs later than the most intense phase of the first, and the maxima near Iceland are eventually more intense than those off Cape Hatteras. Such downstream propagation is consistent with the SST analysis of Hansen and Bezdek (1995), who used higher resolution in space, but lower in time, and did not pinpoint a preferred oscillation time scale.

Anomalies of the same sign as near Iceland, but not as strong, also arise in the tropical Atlantic, off Sierra Leone and, in the most intense phases (3 and 4 or 7 and 8), extending along the west coasts of Africa and Europe to unite with the high-latitude ones. Given the oscillation's peak-to-peak amplitude of up to 0.5 °C in the North Atlantic Drift, its presence in the Central England temperatures over 335 y (Plaut et al. 1995) and the Kochi index of sea-ice extent off Iceland over 370 y (Stocker and Mysak 1992) is not surprising.

The pattern of the shorter-period, 7.5-y oscillation is very different (Fig. 10): anomalies of one sign extend over most of the basin and reach their strongest

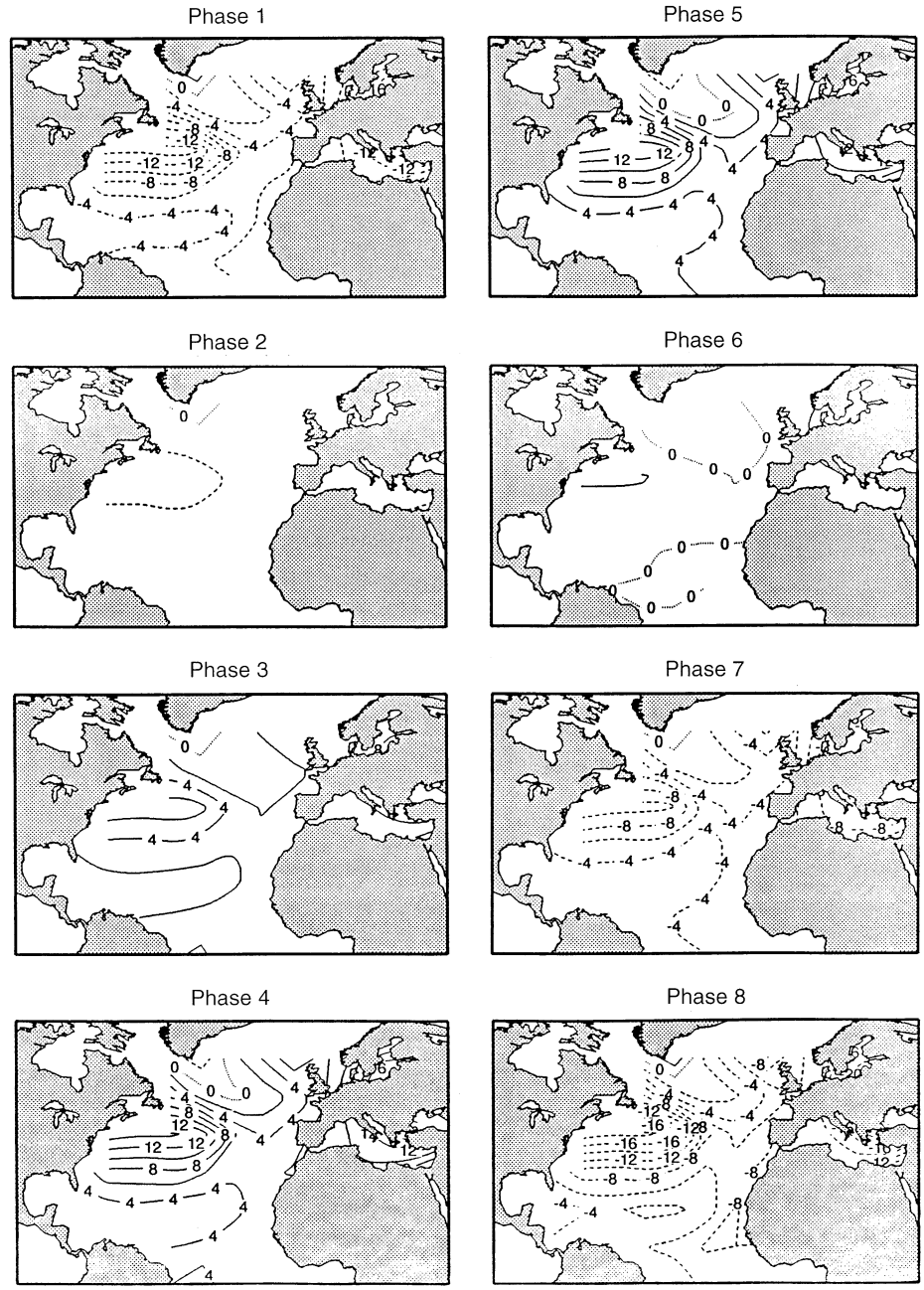

Fig. 10 Same as Fig. 8 but for the 7.5-y oscillation

amplitude over the northwestern part of the subtropical gyre, off New England and Canada's Maritime Provinces, while anomalies of much smaller amplitude and opposite sign occur over the subpolar gyre. Since these SST features, subtropical and subpolar, correlate each in the same way with the intensity of the respective gyre, it appears that the entire double-gyre circulation of the North Atlantic oscillates with this 7.5-y period. The interaction of such an SST oscillation with the atmosphere above (Bjerknes 1964; Deser and Blackmon 1993; Kushnir 1994) and the thermohaline circulation below (Delworth et al. 1993; Chen and Ghil 1995, 1996; McWilliams 1996) deserves further exploration. This peak is also present in global (Ghil and Vautard 1991), as well as in North American (Dettinger et al. 1995b) and European (Plaut et al. 1995) records.

To ascertain further the significance level of these two signals with very low frequency, single-channel MC-SSA was applied, as outlined at the end of Sect. 2.2. The procedure was carried out for S-PCs 1–3 of this domain's SSTs, using $M = 168$. Only components with periods longer than 12 months are retained in the definition of the "deterministic signal." The results of these tests are summarized in Table 5. Note that three levels of significance (80%, 90% and 95%) are considered.

Table 5 Estimation of significance level for channels 1–3 of the North-Atlantic SSTs, using Monte-Carlo SSA (MC-SSA)

Channel	Component (the number in parenthesis is the order of corresponding eigenvalues)	Test: against pure red noise (RN) and against red noise + signal (RN + components)
1	Trend (1–2)	> 95% (RN)
	70–90 months (3–4)	> 95% (RN + 1 − 2)
	68 months (6)	> 80% (RN + 1 − 2)
2	Trend (1)	> 95% (RN)
	160 months (2–3)	> 95% (RN)
	106 months (4)	> 80% (RN)
	50 months (5–6)	> 90% (RN + 1 − 4)
3	Trend (1)	> 95% (RN)
	170 months (2–3)	> 95% (RN)
	25 months (4–5)	> 80% (RN)
	40–60 months (6–7)	> 80% (RN + 1–5)

The interdecadal oscillation, found in channels 2 (with a period of 160 months) and 3 (with 170 months), has a high significance level (95% against red noise). The two channels it affects represent mainly a pattern of phase opposition between the basin's mid-latitudes (and especially the Gulf Stream) with the rest of the North Atlantic. The subdecadal oscillation is highly significant only in channel 1, which depicts the in-phase evolution of the whole basin, with strongest loadings over its western part. Complementary analyses with windows of 240 and 360 months confirm the stability of the 7–8-y spectral peak in this channel. The subdecadal oscillation is significant at the 95% level when tested against a null hypothesis of "red noise + trend" (identified as SSA components 1–2 in channel 1).

For both oscillations, the question arises as to whether these are purely oceanic or coupled, ocean-atmosphere phenomena. Based on 1890–1940 data, Bjerknes (1964) showed that interannual changes in SST are largerly wind-induced, while the long warming trend early this century appears to be driven by ocean-circulation changes (see also Zorita et al. 1992; Deser and Blackmon 1993; Kushnir 1994; Battisti et al. 1995).

The leading mode of interannual atmospheric variability over the round the North Atlantic is the North Atlantic Oscillation (NAO), which describes the intensity of the westerly jet across the domain (Van Loon and Rogers 1978; Rogers 1984). A convenient measure of the NAO is the normalized sea-level pressure (SLP) difference between Ponta Delgada (Azores) and Stykkisholmur (Iceland). This index is available since 1865 on a monthly basis. MC-SSA was performed first on the monthly values of this index between 1865 and 1994, with window widths of 72, 120 and 168 months. No robust oscillations with periods above 12 months stood out. This result is consistent with independent studies of Makrogiannis et al. (1991) on a zonal index over Europe and the Central North Atlantic.

Other studies (Rogers 1984; Kozuchowski 1993; Hurrell 1995; Hurrell and Van Loon 1997) of seasonal or monthly anomalies in SLPs, surface-air temperature and precipitation patterns, however, found interannual and decadal-scale modulations mainly during the boreal winter, when the westerlies reach their strongest intensity. We reanalyzed therefore the NAO index for boreal winter only (December–March) on an interannual basis with window widths of 20 and 30 y. The first component identifies a long-term modulation with stronger westerlies during 1900–1920 and since the 1970s, and weaker westerlies near the beginning of the time series (1870–1890) and even more so during the 1940–1970 interval. A robust oscillation with a period of 7–8 y dominates the interannual variability; its period is close to the one found in SST. This result is consistent with the broad 6–10-y peak in the NAO index of Hurrell and Van Loon (1997).

No significant SSA components are found in this NAO index near 13–15 y. We wished, therefore, to check further the situation for SLPs, representing presumably atmospheric variability, versus SSTs that capture oceanic variability. To do so, we carried out an MSSA analysis of monthly SLPs over the North Atlantic-Western-European area (60 °W–40 °E, 15 °–75 °N), using 6 channels and a windows of $W = 168$ months. Significant peaks appear at 65–86 months (pair 6–7), 56 months (pair 10–11), 32–34 months (pair 8–9), 27 months (pair 15–16), and 9 months (pair 13–14). The latter might be associated with the 7-month peak obtained in a much shorter time series of Gulf Stream variability from satellite data by Lee and Cornillon (1995). Separate analyses for the two intervals preceding and following 1947–1948 confirm the greater strength and robustness of the subdecadal oscillation in the earlier part of the century, as discussed by Deser and Blackmon (1993), but do not reveal a 13–15-y peak either. Ascertaining the nature of ocean-atmosphere coupling, or lack thereof, at subdecadal and interdecadal time scales will clearly require further studies (see

also Cayan 1992; Battisti et al. 1995; Kushinir 1994; Houghton 1996).

4.4 South Atlantic

Only two channels, accounting for 27% of the total variance, are retained. They represent respectively the whole equatorial and southern Atlantic and a seesaw pattern between the NE and SW parts of the basin. Both the long-term trend and decadal variability are strong in the bivariate MSSA and describe together about 40% of the total variance. The spatial aspects of the trend agree with those obtained from the global analysis (Fig. 3) and are therefore not discussed further.

For $W = 168$ months, significant interdecadal variability is present in ST-PCs 2–5. The pair 3–4 does exhibit a spectral peak near 14 years, but does not pass out stringent phase-quadrature test at the preset level (see Sect. 2.2), while Venegas et al. (1996) did find a 15-y peak in this basin's COADS data for 1953–1992, using the multi-taper method. We perform, therefore (see Fig. 11), a reconstruction in channel 1 of both ST-PCs 3–4 and 2–5.

The largest amplitudes occur near the beginning and the end of the century, which could be an end effect of the reconstruction process. Warm episodes are found in 1915–1925, the late thirties, mid-sixties, mid-seventies and late eighties, separated by cold episodes. We also added in Fig. 11 the reconstruction in channel 1 of the North Atlantic's 13–15-year oscillation. Although there are only about seven repetitions of the approximate 13–15-y cycle, the curves in the figure suggest that the North Atlantic leads the South Atlantic by 8 months, with a correlation of 0.48.

As for the interdecadal variability of the North Atlantic, MC-SSA was performed independently on both S-PCs for assessing even more stringently the statistical significance of these interdecadal fluctuations. For channel 1 (in-phase evolution of the whole basin), apart from the long-term trend identified in the first two eigenvalues, which is significant against pure red noise at the 95% level, the other significant components describe the variability related to the 60-month and 40-month peaks (pairs 4–5 and 6–7, respectively), both of which are significant only at the 80% confidence level against the null hypothesis of "red noise + trend". Interdecadal variability associated with the third eigenvalue is not significant in this channel. For channel 2 (seesaw between the equatorial and southeast Atlantic), both the trend (eigenvalue 1) and interdecadal variability (near-equal eigenvalues 2–3) near 13 ys are above the 95% level of significance against pure red noise. The fourth eigenvalue represents very slow variability (strongest peak around 40 y) and is significant at the same level. Interdecadal variability of the South Atlantic is thus highly significant, mainly over the equatorial and SE parts of the basin, as suggested by Mehta and Delworth (1995).

Both QB and lower-frequency interannual oscillations are found in the South Atlantic (see Table 4). There are two well-marked peaks, at 63–65 months and 39–43 months, in the spectrum of the pairs 7–8 ($W = 120$ months) and 8–9 ($W = 168$ months); the second one corresponds to the unique 44-month peak in pair 4–5 of the 72-month window. Using MC-SSA, we also find that the 8–9 pair in the largest window is significant against the null hypothesis of "red noise + signal (1, 2)" for both leading S-PCs. However, the correlation between the associated RCs and their counterpart in the SOI is very weak, suggesting a loss of coherence in the Atlantic's response to ENSO, if any; this result is at variance with the quasi-quadrennial results of Venegas et al. (1996). On the other hand, we find a rather weak cycle, it has a period of 29 months in pair 10–11 for $M = 120$ and of 28 and 33 months in pairs 10–11 and 12–13 for $M = 168$, that might be associated with Latif et al.'s (1996) "Hermanito."

Unal and Ghil (1995) carried out MSSA analyses of tide-gauge data, independently along the eastern and western shores of the Atlantic, but combining the North and South Atlantic, with relative sea-level heights available from 30 °S to 70 °N and 50 °S to 50 °N, respectively. Both analyses give significant peaks at 34 months and 5–8 ys, as well as 15-y modulation of the annual cycle's amplitude along the western shore.

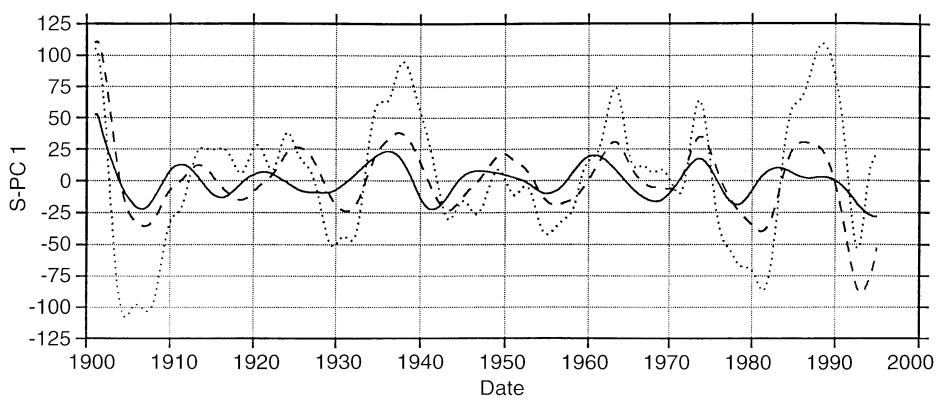

Fig. 11 Reconstructions in the first channel (S-PC 1) of the South-Atlantic components 3–4 (*dashed*) and 2–5 (*dotted*), along with the North-Atlantic 13-y oscillation (*solid*). Units are 0.01 °C

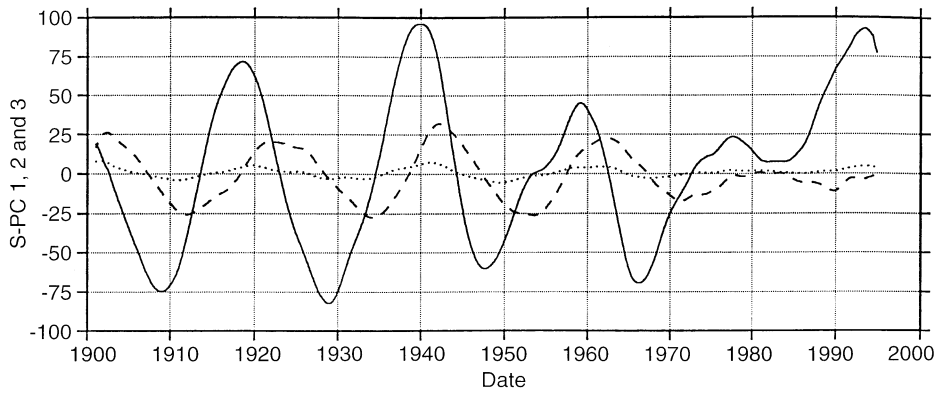

Fig. 12 Reconstruction of the bidecadal components 2–3 in the Indian Ocean, in channels 1, 2 and 3. Units are 0.01 °C

The steric effect of the sea water's density change on sea level is well known (e.g., Roemmich 1990) and the SST results here seem fairly consistent with Unal and Ghil's (1995) results.

4.5 Indian Ocean

Five channels accounting for 33% of total variance are retained. The long-term trend is given by the first MSSA component and represents 20–25% of the total variance, depending on the window used. Subsequent ST-PCs indicate substantial interdecadal variability with no clear pairing into oscillations. ST-PCs 1 to 4 (for $W = 168$ months) peak above 100 months. ST-PCs 2–3 reveal a fairly regular oscillation with a periodicity near 20 y from 1901 till about 1950, which becomes much less regular afterwards (Fig. 12). The variance of RCs 2–3 is largest for channel 1, which describes an in-phase evolution of the whole basin.

MC-SSA with a window of 168 months was carried out for this channel to assess the significance of the lowest-frequency components, as done for the North and South Atlantic basins. The trend (eigenvalue 1, with 51% of the total variance) and the bidecadal component, represented by eigenvalue 2 with a spectral peak at 240 months and 10.7% of total variance, are significant above the 95% level against red noise. When these two components are assigned the role of a "deterministic signal," the bidecadal variability in eigenvalue 3 (also peaking at 240 months) is still significant above the 90% level against "red noise + signal" hypothesis. So a bidecadal oscillation seems significant for the Indian Ocean (Allen et al. 1995).

For $W = 72$ months, no oscillating MSSA pair is detected (see again Table 4). With $W = 120$ months and $W = 168$ months, the Indian Ocean's SSTs do exhibit some paired interannual variability, but the mode that is closest to QB has a period of 34 months (pair 11–12 for $M = 168$). For the lower-frequency mode (pair 6–7 with period 40 months for $M = 120$), lagged correlations of RCs with the corresponding SOI components reach about -0.6. This is consistent with the results of the global analysis in Figs. 5 and 7: high (low) SOI values are associated with cold (warm) anomalies over the whole Indian Ocean, especially throughout its tropical part, which grow during the following six months. For the shorter-period modes, like for the South Atlantic, cross-correlations with similar components of SOI are very weak. So, QB variability recorded in Indian Ocean SSTs seems almost independent from corresponding modes over the Pacific Ocean, when the two domains are analyzed separately.

This SST result seems to contradict the weak but significant correlation between the two tropical basins obtained in zonal surface winds by Barnett (1983, 1991) and Rasmuson et al. (1990). The resolution of this apparent contradiction could lie in ocean-atmosphere coupling that is stronger in the tropical Pacific, on the one hand (see also joint MSSA analyses of SSTs and surface marine winds in Jiang et al. 1995), and the larger cross-basin cohesion of the Walker circulation in the atmosphere, on the other. The latter could also explain, in the absence of such a peak in our SST analyses, indications of a 15–16-month periodicity found in a South-Asian monsoon index (Li 1994; Yanai and Li 1994). This peak is consistent with the Devil's staircase scenario (4/3 y, as found by Jiang et al. 1995 and Robertson et al. 1995 in the Tropical Pacific) and is present in the difference between the 850-mb and 200-mb wind averaged over the region (0–20 °N, 40°–110 °E).

5 Concluding remarks

Space-time variability of sea-surface temperature (SST) fields was analyzed by using multi-channel singular spectrum analysis (MSSA) over the World Ocean and over separate ocean basins. The overall aim was to provide a global picture of observed relationships among these basins' near-surface climate on interannual-to-interdecadal time scales. The length of the UKMO multivariate time series, going back to the beginning of the century, allows the analysis of time scales of 2–15 y. The statistical significance of the regularity of the longest periods in this range is harder

to establish. To do so, Monte-Carlo SSA (MC-SSA) was applied to the leading channels that exhibit the interdecadal periods. Particular attention was paid to the Atlantic Ocean, because of the recent increase of interest in its near- and inter-decadal variability.

The strongest climatic signal is the irregular long-term trend, as found also in other climatic records (Ghil and Vautard 1991; Allen 1992; Folland et al. 1992; Parker et al. 1996). The data-adaptive running means provided by our SSA analyses over the present century confirm (Fig. 4a) the previously noted features, in a slightly smoother version than analyses that had used prescribed weights: a combined gradual increase of SSTs over both southern and northern oceans between 1910 and 1940, a continued increase of NH SSTs through the mid-1950s, while the SH oceans staid colder, a NH cooling through the 1960s and into the late 1970s, while SH SSTs first stay flat and then rise, thus resulting in a reversal of interhemispheric contrast in the early 1970s, and, finally, an SST increase in both hemispheres throughout the 1980s capped by a slight flattering of this long-term trend in recent years.

The short instrumental climate records at our disposal make it difficult to distinguish between explanations of this irregular increase in global SSTs that essentially attempt to interpret it either as a more-or-less monotonic increase or as part of a longer-term, secular oscillation. Gordon (1991) suggests the hypothesis of a long, anomalous "run" of the red-noise processes that drive the low-frequency behavior of the climate system. The most popular "suspects" are anthropogenic greenhouse gases that, barring internal climate variability, would imply a linear increase in SSTs given an exponential increase in carbon dioxide (Dickinson and Cicerone 1986). External forcing has been invoked in the form of slow insolation variations due to the Sun's gradual recovery from the Maunder and Dalton sunspot minima or to its supposed, 80–90 y Gleissberg cycle (Damon and Sonett 1991), as well as to changes in mean terrestrial volcanism on this time scale (Rind and Overpeck 1995). Mann et al. (1995b) have shown evidence for climatic oscillations with a period of about 65years in proxy records extending over up to 500 years, but the shortness of the instrumental SST record we consider, selected for adequate spatial coverage and reliability, prevent us from contributing significantly to this debate.

A novel and striking result here is that large-scale warming and cooling seem to be preceded by similar behavior off the southern tip of Greenland and, soon thereafter, over the Central North Pacific (Fig. 3). This phenomenology suggests an important role for high-latitude processes in the North Atlantic and possible coupling through the atmosphere to the Pacific sector (e.g. Mysak et al. 1990; Chen and Ghil 1996).

On the near-decadal time scale of 7–15 y we did not find regular oscillations with global-scale coherence. Two such oscillations are found to be significant over the North Atlantic, with periods of about 13–15 and 7.5 y. The interdecadal oscillation arises off Cape Hatteras and propagates down the Gulf Stream into the North Atlantic Drift, where its phase is reversed (Fig. 9). In a weakened form, it affects also the tropical Atlantic and leads a similar oscillation in the South Atlantic by about 8 months (Fig. 11). A 13-y oscillation in sea level was found by Unal and Ghil (1995) along the shores of both basins (see also Deser and Blackmon 1993; Hansen and Bezdek 1996; Venegas et al. 1996; Hurrell and Van Loon 1997 for confirmation of various subsets of these results).

Previous evidence for such a signal has been somewhat inconsistent in its spatial pattern or exact periodicity. Allen and Smith (1994) found a 10-y signal that is strongest in the tropical Northern Atlantic, while Mann and Park (1994) and Mehta and Delworth (1995) found an 11–15-y peak with dipolar structure in the tropical Atlantic. A 15-y oscillation found by Ghil and Vautard (1991) in global data sets was shown by Mann and Park (1993) to extend from North America to Southeast Asia and then assigned a period of 15–18 y in later studies of Mann and colleagues (Mann and Park 1994; Mann et al. 1995a, b), while Plaut et al. (1995) found a sharp 14-year peak in Central England temperatures. Sutton and Allen (1997), of which we became aware at revision time, provide some evidence for the North Atlantic that is roughly consistent with our results.

There is considerable interest in the interdecadal variability of ENSO and of related extratropical patterns, such as the Pacific North American (PNA) one (Pan and Oort 1990; Graham 1994; Trenberth and Hurrell 1994; Mann et al. 1995a, b). Our analysis did not detect a major, significant peak at periods longer than 10 years, either over the entire Pacific or the World Ocean. On the other hand, a bidecadal oscillation was detected over the Indian Ocean (as reported by Allen and Smith 1994 and Allan et al. 1995). It is particularly regular in the first half of the century (Fig. 12) and its significance was assessed using MC-SSA on the first channel (S-PCI), which exhibits an in-phase pattern over the whole basin. Such bidecadal variability has also been reported in Indian rainfall by Mitra and Dutta (1992), although we do not agree necessarily with its attribution by these authors to a climatically elusive lunar nodal cycle (see Unal and Ghil 1995 and Currie 1994 for sea-level versus climatic effects of this tidal signal).

Our subdecadal, 7–8 y oscillation involves a phase opposition between the North Atlantic's subtropical and subpolar gyres (Fig. 10). An oscillation with similar period, strongest near Newfoundland, has also been reported by Mann and Park (1994), who associated it with the 7.3-y spectral peak reported in a North-Atlantic Oscillation (NAO) time series by Rogers (1984). We find a significant peak near this frequency using MC-SSA on the boreal-winter NAO index.

On interannual time scales of 2–6 y, three dominant periods have been identified: 24–30, 43 and 60–65 months. The former is the well-known quasi-biennial (QB) component of ENSO, strongest over the tropical Eastern Pacific, with anomalies of the same sign extending along the west coast of the Americas; weaker anomalies, mostly of the opposite sign, cover the rest of the Pacific basin, while the systematic effects in other basins are negligible (Fig. 6). The latter two peaks correspond to Rasmusson et al.'s (1990) low-frequency ENSO component (see also Barnett 1991; Keppenne and Ghil 1992). Jiang et al. (1995), based on 1950–1990 SST and marine surface-wind data from the Tropical Pacific, identified this as a quasi-quadrennial mode.

An important new finding here is that the two apparently distinct low-frequency modes seem to represent a single physical phenomenon, whose frequency shifts fairly abruptly in the 1960s, from near-five years before to near-four years afterwords (Fig. 2; see also Wang and Wang 1996). This fact helps explain the identification of a quasi-quadrennial mode in Jiant et al.'s (1995) data, which covered mostly the latter time interval. The low-but-variable-frequency mode so identified is stronger in the Pacific than the QB one and does extend, albeit with smaller amplitudes, outside the Pacific basin (Fig. 5); their two patterns, when restricted to the Pacific basin, are fairly similar (Figs. 5, 6).

The similarly in spatial pattern between the QB and low-frequency mode, as well as the rather abrupt change in periodicity of the latter, about 4 to 5 y, seems to support the Devil's staircase scenario for ENSO (Jin et al. 1994, 1996; Tziperman et al. 1994; Chang et al. 1995). In this scenario, ENSO irregularity arises from the interaction of the intrinsic instability in the tropical Pacific's coupled ocean-atmosphere system with the seasonal cycle. The shift in frequency noted here might thus be due to frequency locking with an integer multiple of the annual period (see also Jiang et al. 1995 and Robertson et al. 1995). The frequency shift is preceded by a fairly sharp change in SST, and hence thermocline depth, in the tropical Eastern Pacific (Fig. 4b), which plausibly corresponds to the kind of parameter change that induces such frequency shifts in the Devil's terrace (see, in particular, Fig. 6 of Jin et al. 1996).

QB modes are also found in other ocean basins, but they are not correlated at all with the tropical Pacific's Southern Oscillation Index (SOI), or only very weakly so. This suggests that the stronger quasi-quadrennial signal can trigger more easily remote atmospheric forcing outside the Pacific basin (see also Dettinger and Ghil 1997) and then SST response, while the Pacific QB oscillation cannot, or at least not discernibly so. Consistent with previous literature, warm anomalies over the Eastern and Central Pacific are synchronous, in the low-frequency ENSO band, with warm ones along the west coast of the Americas between Alaska and Chile and over the Indian Ocean and with cold anomalies over the equatorial Atlantic (Delecluse et al. 1994; Latif and Barnett 1995), while the Atlantic mid-latitudes are warmer. Warm events are followed 6–12 months later by an overall warming, mostly over the equatorial Atlantic, when El Niño decays in the Tropical Pacific. While low-frequency teleconnections between the tropical Pacific and the Indian Ocean appear to be stable during the current century, it seems that correlations are weaker and less consistent over the Atlantic.

The lagged warming of the equatorial Atlantic almost one year after a Pacific El Niño is clear during the beginnging of the current century and mainly after 1960, when warm events themselves are stronger in amplitude (Gu and Philander 1995). Thus, ENSO oscillations could help trigger similar variability in the equatorial Atlantic, as suggested by Zebiak (1993) and Delecluse et al. (1994), but not be their exclusive cause, since quasi-quadrennial variability in the equatorial and Southern Atlantic is relatively constant during the current century. The modulation of interannual variability around the Atlantic could be due also to other factors, acting on longer time scales. These might include the interhemispheric SST gradient, identified here as part of the global trend (Fig. 4a), or the dipolar structure in the tropical Atlantic identified here in the near-decadal variability (see also Janicot et al. 1996; Trzaska et al. 1996).

A weak oscillation of about 28–30 months is detected in our analysis of the South Atlantic SSTs and is consistent with the "Hermanito" found by Latif et al. (1996), who consider this oscillation to be an analog of the Pacific El Niño. The fact that this mode appears here only with a variance that is lower than the interdecadal and 4–5-y modes, while Latif and colleagues found it to be strongest, could be attributed to the fact that we consider basin-scale SSTs instead of their strictly equatorial index. The time interval analyzed in our study is also longer than in Latif et al. (1996): 1901–1994 here versus 1949–1991 there.

The present results on the spatial patterns of interannual-to-interdecadal oscillations in global and regional SSTs are a step in the comparison of two- and three-dimensional model simulations with observational analyses. Given the current interest in natural climate variability on these time scales (e.g., Martinson et al. 1995), the sharper such comparisons can be made, the faster our progress will be.

Acknowledgements Thanks to David Parker who provided the UKMO data set, to Gregory V, Jones for the NAO index from the University of Virginia, and to Michael Dettinger, Clara Deser, Yochanan Kushnir and Andrew Robertson for fruitful discussions. Some of the programs used here were written by Eric Breitenberger from the University of Alaska, Fairbanks, and others by Guy Plaut at the Université de Nice-Sophia-Antipolis; graphics were produced by the public-domain GMT software. Three anonymous referees provided constructive comments. Gerardo Llamas helped with word processing. M.G.'s work in this area is supported by NSF Grant ATM95-23787. The interaction between the authors was greatly facilitated by M.G.'s residence at LMD as Elf-Aquitaine/C.N.R.S. Professor of the Académie des Sciences for 1996. This is publication

number 4977 of UCLA's Institute of Geophysics and Planetary Physics.

Appendix

Construction of phase composites

Let us denote by $\mathbf{X}(t)$ the state vector containing as coordinates the L leading S-PCs. When two eigencomponents of order k and $k+1$ form an oscillatory pair, their associated ST-PCs $a_k(t)$ and $a_{k+1}(t)$ are in approximate phase quadrature. Following Plaut and Vautard (1994), one calculates the reconstruction. $\mathbf{X}_{k,k+1}(t)$ of the oscillation captured by the two modes, which is a multivariate time series of the same dimension as $\mathbf{X}(t)$. The transform between $\mathbf{X}(t)$ and $\mathbf{X}_{k,k+1}(t)$ is a linear, adaptive filter focusing on the frequency band defined by the modes k and $k+1$. Each scalar component of the vector $\mathbf{X}_{k,k+1}(t)$ has an approximate sinusoidal time behavior, and could therefore be used to define an instantaneous phase index.

Plaut and Vautard (1994) retained, for this purpose, the channel ℓ in which the variance is maximal. A more objective approach is to use the direction in phase space which has a maximal variance; this direction is given by the leading principal component of the reconstruction. Therefore, a new PCA is applied to the multivariate time series $\mathbf{X}_{k,k+1}(t)$, and its first S-PC, $b(t)$, is the time series from which phase and amplitude indices are built. Using this new time series instead of their optimal channel, we then follows the procedure of Plaut and Vautard (1994). Both $b(t)$ and its time derivative $b'(t)$ are normalized, resulting in two new time series $c(t)$ and $c'(t)$, respectively. These time series are, by construction, in approximate phase quadrature. In practice, $c'(t)$ is estimated by centered finite differences.

The phase and amplitude indices, $\theta(t)$ and $A(t)$, can therefore be defined by the argument and the modulus of the complex number $c'(t)+ic(t)$, i.e.,

$$c'(t)+ic(t)=A(t)\mathrm{e}^{i\theta(t)} \tag{A1}$$

In this way one can define objectively the instantaneous state of the oscillation by two real scalars.

Plaut and Vautard (1994) used the high values of $A(t)$ to define spells of intermittent oscillations. Here we focus only on the instantaneous pattern of an oscillation at constant phase, regardless of its amplitude. In order to evaluate this pattern in physical space, we select eight categories (phase 1 to phase 8): the oscillation, at time t is said to belong to "phase m" when

$$(m-1)\frac{\pi}{4}\le\theta(t)\le m\frac{\pi}{4}. \tag{A2}$$

The average of the reconstruction over all occurrences in phase m is called the *phase composite* $\mathbf{C}_m$. It is a vector belonging to the space spanned by the leading L S-EOFs, which can be projected back onto physical space and thus provides the average life cycle of the oscillation's spatial patterns. Figures 5, 6 and 8–10 are constructed in this manner.

References

Aceituno P (1988) On the functioning of the Southern Oscillation in the South American sector. Part I: surface climate. Mon Weather Rev 116:505–524

Allan RJ, Lindesay JA, Reason CJC (1995) Multidecadal variability in the climate system over the Indian Ocean region during the austral summer. J Clim 8:1853–1873

Allen MR (1992) Interaction between the atmosphere and oceans on time scales of weeks to years. PhD Thesis, Clarendon Laboratory, Oxford: 218 pp

Allen MR, Smith LA (1994) Investigating the origins and significance of low-frequency modes of climate variability. Geophys Res Lett 21:883–886

Allen MR, Smith LA (1996) Monte Carlo SSA: detecting irregular oscillations in the presence of colored noise. J Clim 9:3383–3404

Allen MR, Robertson AW (1996) Distinguishing modulated oscillations from colored noise in multivariate datasets. Clim Dyn 12:775–784

Allen MR, Read PL, Smith LA (1992) Temperature time series. Nature 333:686

Barnett TP (1983) Interaction of the monsoon and Pacific trade wind system at interannual time scales. Part I: the equatorial zone. Mon Weather Rev 111:756–773

Barnett TP (1991) The interaction of multiple time scales in the tropical climate system. J Clim 4:269–285

Battisti DS, Bhatt US, Alexander MA (1995) A modeling study of the interannual variability in the wintertime North Atlantic ocean. J Clim 8:3067–3083

Biondi F, Lange CB, Hughes MK, Berger WH (1997) Inter-decadal signals during the last millennium (AD 1117–1992) in the varve record of Santa Barbara basin, California. Geophys Res Lett 24:193–196

Bjerknes J (1964) Atlantic air-sea interaction. Adv Geophys 10:1–82

Bottomley M, Folland CK, Hsiung J, Newell RE, Parker DE (1990) Global ocean surface temperature atlas. HMSO, UK Meteorological Office and Massachusetts Institute of Technology

Broecker WS (1987) Unpleasant surprises in the greenhouse? Nature 321:123–126

Broomhead DS, King GP (1986a) Extracting qualitative dynamics from experimental data. Physica D 20:217–236

Broomhead DS, King GP (1986b) On the qualitative analysis of experimental dynamical systems. In: Sarkar S (ed) Nonlinear phenomena and chaos. Adam Hilger, Bristol, pp 113–144

Cayan DR (1992) Latent and sensible heat flux anomalies over the Northern Oceans: driving the sea surface temperature. J Phys Oceanogr 22:859–881

Chang P, Ji L, Wang B, Li T (1995) Interactions between the seasonal cycle and El Niño-Southern Oscillation in an intermediate coupled ocean-atmosphere model. J Atmos Sci 52:2353–2372

Chen F, Ghil M (1995) Interdecadal variability of the thermohaline circulation and high-latitude surface fluxes. J Phys Oceanogr 25:2547–2568

Chen F, Ghil M (1996) Interdecadal variability in a hybrid coupled ocean-atmosphere model. J Phys Oceanogr 26:1561–1578

Cook ER (1995) Temperature histories from tree rings and corals. Clim Dyn 11:211–222

Currie RG (1994) Variance contribution of luni-solar cycle signals in the St Lawrence and Nile river records. Int J Climatol 14:843–852

De Costa E, Vautard R (1996) A qualitatively realistic low-order model of the extratropical low-frequency variability built from long records of potential vorticity. J Atmos Sci 54:1064–1084

Damon PE, Sonett CP (1991) Solar and terrestrial components of the atmospheric 14C variation spectrum. In: Sonett CP, Giampapa MS, Matthews MS (eds) The Sun in time. The University of Arizona Press, pp 360–388

Delecluse P, Servain J, Levy C, Arpe K, Bengtsson L (1994) On the connection between the 1984 Atlantic warm event and the 1982–83 ENSO. Tellus 46A:448–464

Delworth T, Manabe S, Stouffer RJ (1993) Interdecadal variations of the thermohaline circulation in a coupled ocean-atmosphere model. J Clim 6:1993–2001

Deser C, Blackmon ML (1993) Surface climate variations in the North Atlantic ocean during winter: 1900–1989. J Clim 6:1743–1753

Dettinger MD, Ghil M (1998) Seasonal and interannual variations of atmospheric CO_2 and climate. Tellus 50 (B) 1–24

Dettinger MD, Ghil M, Strong C, Weibel W, Yiou P (1995a) Software expedites singular-spectrum analysis of noisy time series. Eos Trans AGU 76:12, 14, 21

Dettinger MD, Keppenne CL, Ghil M (1995b) Interannual and interdecadal variability in United States surface-air temperatures, 1910–87. Clim Change 31 : 35–66
Dickson RE, Cicerone RJ (1986) Future global warming from atmospheric trace gases. Nature 319 : 109–115
Elsner JB, Tsonis AA (1991) Do bidecadal oscillations exist in the global temperature record? Nature 353 : 551–553
Elsner JB, Tsonis AA (1994) Low-frequency oscillation. Nature 372 : 507–508
Folland CK, Parker DE (1995) Correction of instrumental biases in historical sea surface temperature data. J Meteorol Soc 121 : 319–368
Folland CK, Palmer TN, Parker DE (1986) Sahel rainfall and worldwide sea surface temperature. Nature: 602–607
Folland CK et al. (1992) Observed climate variability and change. In: JT Houghton et al. (eds) Climatic change 1992. Supplement to the IPCC scientific assessment, Cambridge University Press, Cambridge, UK, Chapter C, pp 135–170
Fritts HC, Lofgren CGR, Gordon GA (1979) Variations in climate since 1602 as reconstructed from tree-rings. Quatern Res 12 : 18–46
Ghil M, Vautard R (1991) Interdecadal oscillations and the warming trend in global temperature time series. Nature 350 : 324–327
Ghil M, Yiou P (1996) Spectral methods: What they can and cannot do for climatic time series. In: Anderson D, Willebrand J (eds) Decadal climate variability and predictability. Elsevier, Amsterdam pp 446–482
Ghil M, Taricco C (1997) Advanced spectral analysis methods. In: Cini Castagnoli G, Provenzale A (eds) Past and present variability of the solar-terrestrial system: measurement, data analysis and theoretical models. Società Italiana di Fisica, Bologna, and IOS Press, Amsterdam, pp. 137–159
Ghil M, Mullhaupt A, Pestiaux P (1987) Deep water formation and quaternary glaciations. Clim Dyn 2 : 1–10
Gordon AH (1991) Global warming as a manifestation of a random walk. J Clim 6 : 589–597
Graham NE (1994) Decadal scale climate variability in the tropical and North Pacific during the 1970's and 1980's: observations and model results. Clim Dyn 10 : 135–162
Greatbatch RJ, Zhang S (1995) An interdecadal oscillation in an idealized ocean basin forced by constant heat flux. J Clim 8 : 81–91
Gu D, Philander SGH (1995) Secular changes of annual and interannual variability in the Tropic during the past century. J Clim 8 : 864–876
Hansen DV, Bezdek HF (1996) On the nature of decadal anomalies in North Atlantic sea surface temperature. J Geophys Res 101 : 8749–8758
Hasselmann K (1976) Stochastic climate models, Part I: Theory. Tellus 28 : 473–485
Hasselmann K (1988) PIPs and POPs: The reduction of complex dynamical systems using principal interaction and principal oscillation patterns. J Geophys Res 93D : 11015–11021
Hastenrath S, Covey A (1978) The Pacific El-Niño phenomenon and the Atlantic circulation. Q J R Meteorol Soc 103 : 77–92
Houghton RW, Tourre Y (1992) Characteristics of low frequency sea surface temperature fluctuations in the tropical Atlantic. J Clim 5 : 765–771
Houghton JT, Jenkins GJ, Ephraums JT (eds) (1990) Climte change. The IPCC scientific assessment, Cambridge University Press, Cambridge, UK
Houghton RW (1996) Subsurface quasi-decadal fluctuations in the North Atlantic. J Clim 9 : 1363–1373
Hurrell JW (1995) Decadal trends in the North Atlantic Oscillation: regional temperatures and precipitation. Science 269 : 676–679
Hurrell JW (1996) Influence of variations in extratropical wintertime teleconnections on Northern Hemisphere temperature. Geophys Res Lett 23 : 665–668
Hurrell JW, Van Loon H (1997) Decadal variations in climate associated with the North Atlantic Oscillation. Clim Change 36 : 301–326
Janicot S, Moron V, Fontaine B (1996) Sahel droughts and ENSO dynamics. Geophys Res Lett 23 : 551–554
Jiang N, Neelin JD, Ghil M (1995) Quasi-quadrennial and quasi-biennial variability in the equatorial Pacific. Clim Dyn 12 : 101–112
Jin FF, Neelin JD, Ghil M 1(1994) El Niño on the devil's staircase: annual subharmonics steps to chaos. Science 264 : 70–72
Jin FF, Neelin JD, Ghil M (1996) El Niño/Southern Oscillation and the annual cycle: Subharmonic frequency-locking and aperiodicity. Physica D 98 : 442–465
Jones PD, Raper SCB, Bradley RS, Diaz HF, Kelly PM, Wigley TML (1986a) Northern Hemisphere surface air temperature variations 1851–1984. J Clim Appl Meteorol 25 : 161–179
Jones PD, Raper SCB, Bradley RS, Diaz HF, Kelly PM, Wigley TML (1986b) Southern Hemisphere surface air temperature variations 1851–1984. J Clim Appl Meteorol 25 : 1213–1220
Kawamura (1994) A rotated EOF analysis of global interannual and interdecadal scales. J Phys Oceanogr 24 : 707–715
Keppenne CL, Ghil M (1992) Adaptive filtering and prediction of the Southern Oscillation index. J Geophys Res 97 : 20449–20454
Keppenne CL, Ghil M (1993) Adaptive filtering and prediction of noisy multivariate signals: an application to subannual variability in atmospheric angular momentum. Int J Bifurcation Chaos 3 : 625–634
Kerr RA (1994) Did the tropical Pacific drive the world's warming? Science 266 : 544–545
Kimoto M, Ghill M, Mo KC (1991) Spatial structure of the 40-day oscillation in the Northern Hemisphere extratropics. Proc 8th Conf Atmospheric and Oceanic Waves and Stability. American Meteorological Society, Boston, pp 115–116
Kozuchowski KM (1993) Variations of hemispheric zonal index since 1899 and its relationship with air temperature. Int J Climatol 13 : 853–864
Kumar A, Leetma A, Ji M (1996) Simulations of atmospheric variability induced by sea surface temperature and implications for global warming. Science 266 : 632–634
Kushnir Y (1994) Interdecadal variations in the North Atlantic sea surface temperature and associated atmospheric conditions. J Clim 7 : 141–157
Lanzante JR (1996) Lag relationships involving tropical sea surface temperatures. J Clim 9 : 2568–2578
Latif M, Barnett TP (1994) Causes of decadal climate variability over the North Pacific and North America. Science 266 : 634–637
Latif M, Barnett TP (1995) Interactions of the tropical oceans. J Clim 8 : 952–964
Latif M, Groetzner A, Frey H (1996) El Hermanito: El Niño's little brother in the Atlantic. Max-Planck Institut für Meteorologie, Report No 196
Lau KM, Sheu PJ (1988) Annual cycle, quasi-biennial oscillation and Southern Oscillation in global precipitation. J Geophys Res 93 : 10975–10988
Lau KM, Weng H (1995) Climate signal detection using wavelet transform: how to make a time series sing. Bull Am Meteorol Soc 76 : 2391–2403
Lee T, Cornillon P (1995) Temporal variation of meandering intensity and domain-wide lateral oscillations of the Gulf Stream. J Geophys Res 100 : 13603–13613
Li C (1994) Interannual variability of the Asian Summer Monsoon and its relationships with ENSO and Eurasian snow cover. PhD Thesis, Department of Atmospheric Sciences, University of California, Los Angeles, 197 pp
Liang XZ, Samel AN, Wang WC (1995) Observed and GCM simulated decadal variability of monsoon rainfall in East China. Clim Dyn 11 : 103–114
Mak M (1995) Orthogonal wavelet analysis: interannual variability in the sea surface temperature. Bull Am Meteorol Soc 76 : 2179–2186
Makrogiannis TJ, Sahsammanoglu HS, Flocas AA, Bloutsos AA (1996) Analysis of the monthly zonal index values and longer-term changes of circulation over the North Atlantic and Europe. Int J Climatol 11 : 493–503
Manley G (1953) The mean temperature of central England, 1698–1952. Q J R Meteorol Soc 79 : 242–261

Manley GQ (1974) Central England temperatures: monthly means 1659 to 1973. Q J R Meteorol Soc 100 : 389–405
Mann ME, Park J (1993) Spatial correlations of interdecadal variation in global surface temperatures. Geophys Res Lett 20 : 1055–1058
Mann ME, Park J (1994) Global-scale modes of surface temperature variability on interannual to century timescales. J Geophys Res 99 : 25819–25833
Mann ME, Park J (1996) Joint spatiotemporal modes of surface temperature and sea level pressure variability in the Northern Hemisphere during the last century. J Clim 9 : 2137–2162
Mann ME, Lall U, Saltzman B (1995a) Decadal to centennial scale climate variability: insights into the rise and fall of the Great Salt Lake. Geophys Res Lett 22 : 937–940
Mann ME, Park J, Bradley RS (1995b) Global interdecadal and century-scale climate oscillations during the five post centuries. Nature 378 : 266–270
Martinson DG, Bryan K, Ghil M, Hall MM, Karl TR, Sarachik ES, Sorooshian S, Talley LD (eds) (1995) Natural climate variability on decade-to-century time scales. National Academy Press, Washington, DC, 630 pp
McWilliams JC (1996) Modelling the oceanic general circulation. Annu Rev Fluid Mech 28 : 215–248
Meehl GA (1987) The annual cycle and its relationship to interannual variability in the tropical Pacific and Indian ocean regions. Mon Weather Rev 115 : 27–50
Meehl GA (1992) A coupled air-sea biennial mechanism in the tropical Indian and Pacific regions: role of the ocean. J Clim 6 : 31–41
Mehta VM, Delworth T (1995) Decadal variability of the tropical Atlantic Ocean surface temperature in shipboard measurements and in a global ocean atmosphere model. J Clim 8 : 172–190
Meyers SD, Kelly BG, O'Brien JJ (1993) An introduction to wavelet analysis in oceanography and meteorology: with application to the dispersion of Yanai waves. Mon Weather Rev 121 : 2858–2866
Mitra K, Dutta SN (1992) 18.6 luni-solar nodal and 10–11 y solar signals in rainfall in India. Int J Climatol 12 : 839–852
Molinari RL, Mayer DA, Festa JF, Bezdek HF (1997) Multiyear variability in the near-surface temperature structure of the midlatitude western North Atlantic Ocean. J Geophys Res 102 : 3267–3278
Moron V (1997) Trend, decadal and interannual variability in annual rainfall in subequatorial and tropical North Africa (1900–1994). Int J Climatol 17 : 785–806
Moron V, Fontaine B, Roucou P (1995) Global equatorial variability of 850 and 200 hPa zonal winds from rawinsondes between 1963 and 1989. Geophys Res Lett 23 : 1701–1704
Mysak LA, Manak DK, Marsden RF (1990) Sea-ice anomalies observed in the Greenland and Labrador Seas during 1901–1984 and their relation to an interdecadal Arctic climate cycle. Clim Dyn 5 : 111–113
Mysak LA, Peng S, Wood RG (1991) Application of a coupled ice-ocean model to the Labrador Sea. Atmosphere-Ocean 29 : 232–255
Neelin JD, Jin F-F (1993) Modes of interannual tropical ocean-atmosphere interaction — a unified view. Part II: analytical results in the weak-coupling limit. J Atmos Sci 50 : 3504–3522
Nicholls N, Gruza GV, Jouzel J, Karl TR, Ogallo LA, Parker DE (1996) Observed climate variability. In: JT Houghton, LG Meira Filho, BA Callander, N Harris, A Kattenberg, K. Maskell (eds) Climatic change 1995: the science of climate change. Cambridge University Press, Cambridge, UK, pp 133–192
Nicholson SE, Entekhabi D (1986) The quasi-periodic behavior of rainfall variability in Africa and its relationship to the Southern Oscillation. Arch Meteorol Geophys Biocl 34A : 311–348
O'Lenic EA, Livezey RE (1988) Practical considerations in the use of rotated principal component analysis (RPCA) in diagnostic studies of upper-air height fields. Mon Weather Rev 116 : 1682–1689
Ooms M (1988) Empirical vector autoregressive modeling, Springer-Verlag, Berlin Heidelberg, New York
Pan YH, Oort AH (1990) Correlation analyses between SST anomalies in the Eastern equatorial Pacific and the World Ocean. Clim Dyn 4 : 191–205
Parker DE, Jones PD, Folland CK, Bevan A (1994) Interdecadal changes of surface temperature since the late nineteenth century. J Geophys Res 99 : 14373–14399
Parker DE, Horton EB, Cullum DPN, Folland CK (1996) Global and regional climate in 1995. Weather 51 : 202–209
Parthasarathy B, Rupa Kumar K, Munto AA (1993) Homogenous Indian monsoon rainfall: variability and prediction. Proc Ind Acad Sci (Earth Planet Sci) 102 : 121–155
Penland C (1996) A stochastic model of IndoPacific sea surface temperature anomalies. Physica D 98 : 534–558
Penland C, Ghil M (1993) Forecasting Northern Hemisphere 700-mb geopotential height anomalies using empirical normal modes. Mon Weather Rev 121 : 2355–2372
Philander SGH (1990) El Niño, and the Southern Oscillation, Academic Press, San Diego, 293 pp
Pisciottano G, Díaz A, Cazes G, Mechoso CR (1994) El Niño-Southern Oscillation impact on rainfall in Uruguay. J Clim 7 : 1286–1302
Plaut G, Vautard R (1994) Spells of low-frequency oscillations and weather regimes in the Northern Hemisphere. J. Atmos Sci 51 : 210–236
Plaut G, Ghil M, Vautard R (1995) Interannual and interdecadal variability in 335 years of Central England temperature. Science 268 : 710–713
Quinn M, Crowley TJ, Taylor FW (1996) New stable isotope results from a 173-year coral from Espiritu Santo, Vanuatu. Geophys Res Lett 23 : 3413–3416
Rahmstorf S (1995) Bifurcations of the Atlantic thermohaline circulation in response to change in hydrological cycle. Nature 378 : 145–149
Rasmuson EM, Carpenter T (1982) Variations in tropical sea surface temperature and surface winds associated with the Southern Oscillation/El Niño. Mon Weather Rev 110 : 354–384
Rasmuson EM, Wang X, Ropelewski CF (1990) The biennial component of ENSO variability. J Mar Syst 1 : 71–96
Read JF, Gould WJ (1992) Cooling and freshening of the subpolar North Atlantic ocean since the 1960s. Nature 360 : 55–57
Rind DH, Overpeck JT (1995) Modeling the possible causes of decadal-to-millenial-scale variability. In: Martinson DG, Bryan K, Ghil M, Hall MM, Karl TR, Sarachik ES, Sorooshian S, Talley LD (eds) Natural climate variability on decadal-to-century time scales. National Academy Press, Washington, DC : PP 187–197
Robertson AW, Ma CC, Ghil M, Mechoso CR (1995) Simulation of the tropical-Pacific climate with a coupled ocean-atmosphere general circulation model. Part II: interannual variability. J Clim 8 : 1199–1216
Roemmich D (1990) Sea level and thermal variability of the oceans. Sea-level change. National Academy Press, Washington D.C., pp 208–217
Rogers JC (1984) The association between the North Atlantic Oscillation and the Southern Oscillation in the Northern Hemisphere. Mon Weather Rev 112 : 1999–2015
Ropelewski CF, Halpert MS (1987) Global and regional scale precipitation associated with El Niño/Southern Oscillation. Mon Weather Rev 115 : 1606–1626
Ropelewski CF, Halpert MS, Wang X (1992) Observed tropospheric biennial variability and its relation to the Southern Oscillation. J Clim 5 : 594–614
Schlesinger ME, Ramankutty N (1994a) An oscillation in the global climate system of period 65–70 years. Nature 367 : 723–726
Schlesinger ME, Ramankutty N (1994b) Reply to "Low-frequency oscillation" by Elsner JB and Tsonis AA (1994). Nature 372 : 508–509
Schlesinger ME, Ramankutty (1995) Is the recently reported 65- to 70-year surface temperature oscillation the result of climate noise? J Geophys Res 100 : 13767–13774

Schlosser P, Bönisch G, Rhein M, Bayer R (1991) Reduction of deepwater formation in the Greenland Sea during the 1980s: evidence from tracer data. Science 251 : 1054–1056

Servain J (1991) Some simple climatic indices for the tropical Atlantic Ocean and some application. J Geophys Res 96 : 15137–15146

Speich S, Dijkstra H, Ghil M (1995) Successive bifurcations in a shallow-water model, applied to the wind-driven ocean circulation. Nonlin Proc Geophys 2 : 241–268

Stocker TF, Mysak LA (1992) Climatic fluctuations on the century time scale: a review of high-resolution proxy data and possible mechanisms. Clim Change 20 : 227–250

Sutton RT, Allen MR (1997) Decadal predictability of North Atlantic sea surface temperature and climate. Nature 388 : 563–567

Tanimoto Y, Iwasaka N, Hanawa K, Toba Y (1993) Characteristic variations of SST with multiple time scales in the North Pacific. J Clim 6 : 1153–1160

Terry P (1995) Space-time structure of monsoon interannual variability. J Clim 8 : 2595–2619

Trenberth KE (1990) Recent observed interdecadal climate changes in the Northern Hemisphere. Bull Am Meteorol Soc 71 : 988–993

Trenberth KE, Hurrel JW (1994) Decadal atmosphere-ocean variations in the Pacific. Clim Dyn 9 : 267–319

Trzaska S, Moron V, Fontaine B (1996) Global atmospheric response to specific linear combination of the main SST modes. Part I: numerical experiments and preliminary results. Ann Geophys 14 : 1066–1078

Tziperman E, Stone L, Cane M, Jarosh H (1994) El Niño chaos: overlapping of resonances between the seasonal cycle and the Pacific ocean-atmosphere oscillator. Science 264 : 72–74

Unal YS, Ghil M (1995) Interannual and interdecadal oscillation patterns in sea level. Clim Dyn 11 : 255–278

Van Loon H, Rogers JC (1978) The seesaw in winter temperatures between Greenland and northern Europe, Part I: general description. Mon Weather Rev 106 : 296–310

Vautard R, Ghil M (1989) Singular Spectrum Analysis in nonlinear dynamics with applications to paleoclimatic time series. Physica D 35 : 395–424

Vautard R (1995) Patterns in time: SSA and MSSA. In: von Storch H, Navarra A (eds) Analysis of climate variability. Springer-Verlag Berlin Heidelberg, New York pp 259–278

Vautard R, Yiou P, Ghil M (1992) SSA: a toolkit for short noisy chaotic time series. Physica D 58 : 95–126

Venegas SA, Mysak LA, Straub DN (1996) Evidence for interannual and interdecadal climate variability in the South Atlantic. Geophys Res Lett 23 : 2673–2676

von Storch H, Bruns T, Fischer-Bruns I, Hasselman K (1988) Principal oscillation pattern analysis of the 30- to 60-day oscillation in general circulation model equatorial troposphere. J Geophys Res 9 : 11022–11036

Wang B (1995) Interdecadal changes in El Niño onset in the last four decades. J Clim 8 : 267–285

Wang B, Ropelewski CF (1995) An assessment of ENSO-scale secular variability. J Clim 8 1584–1599

Wang B, Wang Y (1996) Temporal structure of the SOI as revealed by waveform and wavelet analysis. J Clim 9 : 1586–1598

Weaver AJ, Sarachik ES, Marotzke J (1991) Freshwater flux forcing of decadal and interdecadal variability. Nature 353 : 836–838

Weisse R, Mikolajewicz U, Maier-Reimer E (1994) Decadal variability of the North Atlantic in an ocean general circulation model. J Geophys Res 99 : 12411–12421

Woodruff SDR, Slutz RJ, Jenne RL, Steurer PM (1987) A comprehensive ocean-atmosphere data set. Bull Am Meteorol Soc 68 : 521–527

Yanai M, Li C (1994) Interannual variability of the Asian summer monsoon and its relationship with ENSO, Eurasian snow cover and heating. Proc Int Conf Monsoon Variability and Prediction. International Centre for Theoretical Physics, Trieste, Italy, 9–13 May: pp 27–34

Yiou P, Jouzel J, Johnsen S, Rögnvaldsson ÖE (1995) Rapid oscillations in Vostok and GRIP ice cores. Geophys Res Lett 22 : 2179–2182

Yiou P, Baert E, Loutre MF (1996) Spectral analysis of climate data. Surveys Geophys 17 : 619–663

Zebiak S (1993) Air-sea interaction in the equatorial Atlantic region. J Clim 6 : 1567–1586

Zhang Y, Wallace JM, Battisti DS (1997) ENSO-like interdecadal variability: 1900–1993. J Climate (in press)

Zorita Z, Kharin V, Von Storch H (1992) The atmospheric circulation and sea surface temperature in the North Atlantic area in winter: their interaction and relevance to Iberian precipitation. J Clim 5 : 1097–1108

Zwiers FW, von Storch H (1995) Taking serial correlation into account in tests of the mean. J Clim 8 : 336–351